nature cell biology

Coupling between hydrodynamic forces and planar cell polarity orients mammalian motile cilia

Boris Guirao[1,2,7], Alice Meunier[1,7], Stéphane Mortaud[1], Andrea Aguilar[1], Jean-Marc Corsi[1], Laetitia Strehl[1], Yuki Hirota[3], Angélique Desoeuvre[4], Camille Boutin[4], Young-Goo Han[5], Zaman Mirzadeh[5], Harold Cremer[4], Mireille Montcouquiol[6,8], Kazunobu Sawamoto[3,8] and Nathalie Spassky[1,9]

In mammals, motile cilia cover many organs, such as fallopian tubes, respiratory tracts and brain ventricles. The development and function of these organs critically depend on efficient directional fluid flow ensured by the alignment of ciliary beating. To identify the mechanisms involved in this process, we analysed motile cilia of mouse brain ventricles, using biophysical and molecular approaches. Our results highlight an original orientation mechanism for ependymal cilia whereby basal bodies first dock apically with random orientations, and then reorient in a common direction through a coupling between hydrodynamic forces and the planar cell polarity (PCP) protein Vangl2, within a limited time-frame. This identifies a direct link between external hydrodynamic cues and intracellular PCP signalling. Our findings extend known PCP mechanisms by integrating hydrodynamic forces as long-range polarity signals, argue for a possible sensory role of ependymal cilia, and will be of interest for the study of fluid flow-mediated morphogenesis.

Motile cilia constitute a widespread and efficient tool that allow motion of microorganisms such as *Paramecium*[1], or that generate fluid flow above ciliated epithelia. They cover organs such as fallopian tubes, respiratory tracts and brain ventricles. Ciliary dysfunction may result in severe diseases, including situs inversus, infertility, bronchiectasis or ectopic pregnancy[2–5]. In the brain, motility defects in ependymal cilia covering ventricular walls cause hydrocephalus[4,6,7] and alter migration of neuroblasts toward the olfactory bulb[8].

Generation of cilia-powered directional fluid flow at the tissue level requires orientation of their beating in a common direction[8–10]. Mechanisms governing ciliary orientation during development significantly differ between species. In *Paramecium*, ciliary orientation of daughter cells is inherited from the mother cell[11,12]. In quail oviduct epithelium, graft experiments showed that cilia orientation is set before differentiation[13]. In *Xenopus laevi* larvae skin, a two-step process has been identified: first, patterning occurring after gastrulation biases orientation of basal bodies within a window of 180° when they dock at the membrane; second, basal bodies refine their orientation in response to the fluid flow created by the oriented beating of their cilia[14].

Polarization of cells in the apical plane is known to be instructed by the PCP pathway[15]. Accordingly, the patterning observed in *Xenopus* has been shown to involve PCP proteins[16] and to be driven by neighbouring mucosal epithelial cells through a non-cell-autonomous PCP pathway[17]. In mammals, this pathway is involved in the planar orientation of subcellular[18] and multicellular structures[19], with respect to the body axis. Core proteins involved in this signalling pathway were first described in *Drosophila melanogaster*, and seem to be conserved in mammals[20]. However, the cues instructing the initial direction of polarization and its long-range spreading over the tissue remain obscure[21].

In mammals, the mechanisms involved in the ciliary orientation process are still entirely unknown despite the importance of proper cerebrospinal fluid (CSF) flow in brain development[6–8]. Therefore, we studied orientation of ciliary beating in ependymal cells during mouse brain development. By combining biophysical and molecular approaches, we show that mammalian cilia orientation requires an original mechanism that couples fluid flow and the PCP protein Vangl2. Our findings thus identify a direct link between hydrodynamic forces and intracellular PCP signalling, and uncover a new type of PCP mechanism that integrates external cues from hydrodynamic forces.

RESULTS

Progressive alignment of ependymal cilia during development

In the adult mouse brain, the direction of ciliary beating follows the direction of local CSF flow, which they help propel[8] (Fig. 1e;

[1]Institut de Biologie de l'Ecole Normale Supérieure (IBENS), Institut National de la Santé et de la Recherche Médicale U1024, Centre National de la Recherche Scientifique UMR8197, 75005 Paris, France. [2]Laboratoire Physico-chimie Curie, UMR 168, Institut Curie, 75248, Paris, France. [3]Department of Developmental and Regenerative Biology, Institute of Molecular Medicine, Nagoya City University Graduate School of Medical Sciences, Nagoya 467-8601, Japan. [4]IBDML, CNRS/Université de Méditerranée, Campus de Luminy, Marseille, France. [5]Department of Neurological Surgery, University of California San Francisco, San Francisco, CA 94143, USA. [6]INSERM, U862, Neurocentre Magendie, Molecular Basis of Planar Polarity group, Bordeaux, F-33000, Université de Bordeaux, Bordeaux, F-33000, France.
[7,8]These authors contributed equally to this work.
[9]Correspondence should be addressed to N.S. (e-mail: spassky@biologie.ens.fr)

Received 25 January 2010; accepted 4 March 2010; published online 21 March 2010; corrected online 26 March 2010; DOI: 10.1038/ncb2040

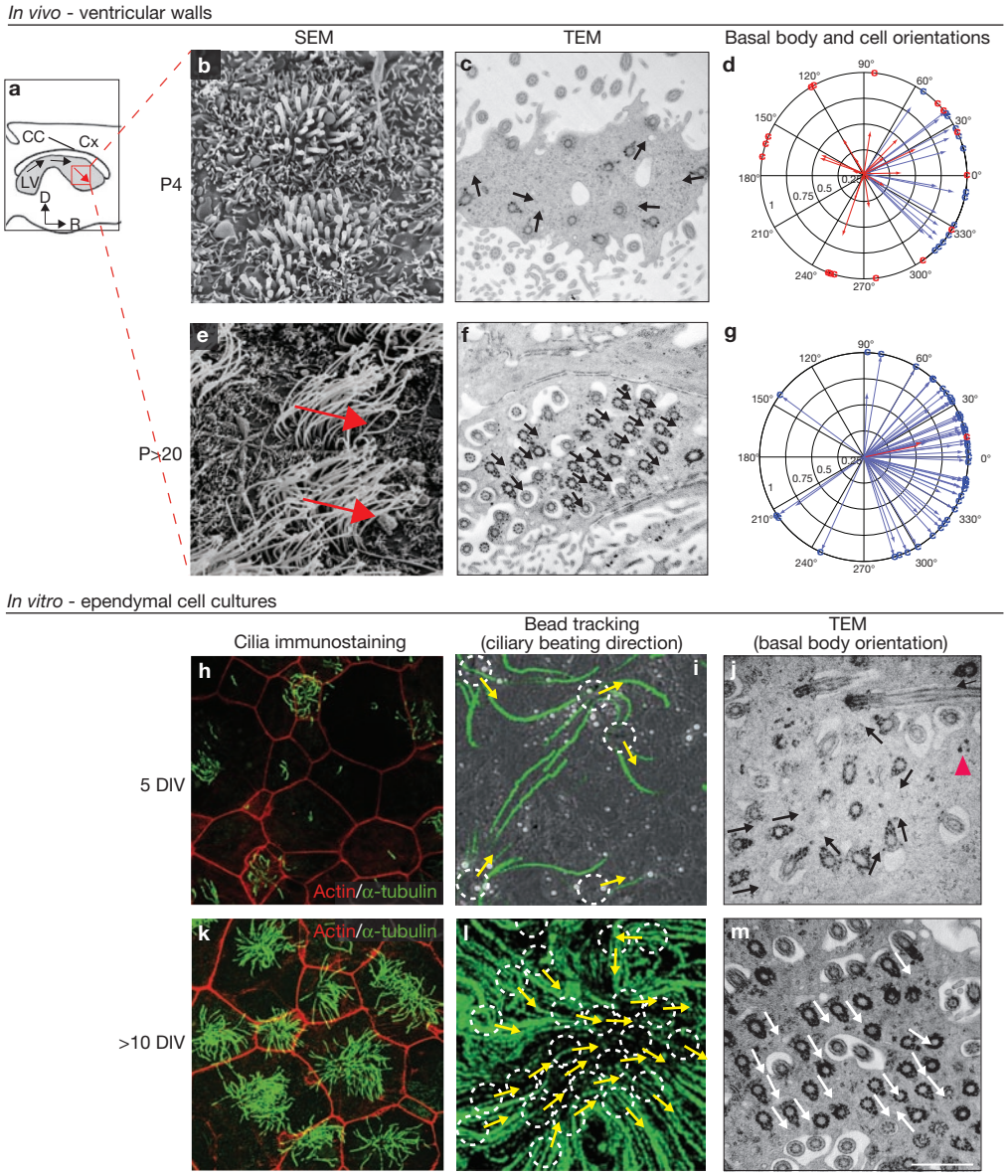

Figure 1 Progressive orientation of ependymal cilia during development. (**a**) Schematic sagittal view of a mouse lateral ventricular wall. Ciliary beating directions at three caudo-rostral levels are indicated (arrows)[8]. The red square indicates the region analysed in **b**–**g** (CC, corpus callosum; Cx, cortex; LV, lateral ventricle; R, rostral; D, dorsal). (**b**, **e**) SEM of multiciliated cells showing preferential direction at P21 (red arrows). (**c**, **f**) TEM of cell transverse sections showing basal feet directions (arrows). (**d**, **g**) Quantification of basal feet directions in P4 (305 basal bodies in 30 cells from 2 mice, **d**) and P21 (563 basal bodies in 49 cells from 2 mice, **g**) mice. Arrows point in the mean direction of basal feet in each cell; arrow length r_{Cell} quantifies their alignment. Red arrows represent cells with random basal feet distribution (see Supplementary Information, Figs S2–4). (**h**–**m**) Primary culture of multiciliated ependymal cells at 5 DIV (**h**–**j**) and 10 DIV (**k**–**m**). (**h**, **k**) Cilia and cell borders are stained with detyrosinated α-tubulin (1D5, green) and phalloidin (red) antibodies, respectively. One cluster of cells is shown in **k**. (**i**, **l**) Superposition of phase-contrast and fluorescent microscopy images. (**i**) Bead trajectories (green) follow the flow generated by ciliary beatings (yellow arrows) of each multiciliated cell (dashed circles). (**l**) Bead trajectories follow the flow generated by ciliary beatings of a single cluster of about 20 cells. (**j**, **m**) TEM of cell transverse sections showing basal feet directions (arrows). Scale bars, 2.5 μm (**b**), 5 μm (**e**), 1.4 μm (**c**, **f**), 20 μm (**h**, **i**, **k**, **l**) and 1 μm (**j**, **m**).

Supplementary Information, Fig. S1). Multiciliated ependymal cells are derived from radial glial cells during embryonic development[22]. Their maturation starts at early postnatal stages and is characterized by growth of cilia from basal bodies docked at their apical membrane. At postnatal day 4 (P4) these cells are widely distributed along the ventricular walls; however, most of them are still immature, as shown by their short cilia[22] (Fig. 1b). Using transmission electron microscopy (TEM), we identified three stages of ependymal cell maturation. Stage 1 cells show multiple deuterosomes assembling basal bodies deep in the cytoplasm (Supplementary Information, Fig. S2a). Stage 2 cells contain 'old' deuterosomes and young basal bodies (Supplementary Information, Fig. S2b, d–f) docked at their apical surface (Supplementary Information, Fig. S3a). Stage 3 cells show 'mature' basal bodies and no deuterosome (Supplementary Information, Fig. S2c). We quantified ciliary orientation at P4 by scoring orientations of putative or identified basal feet, which are basal

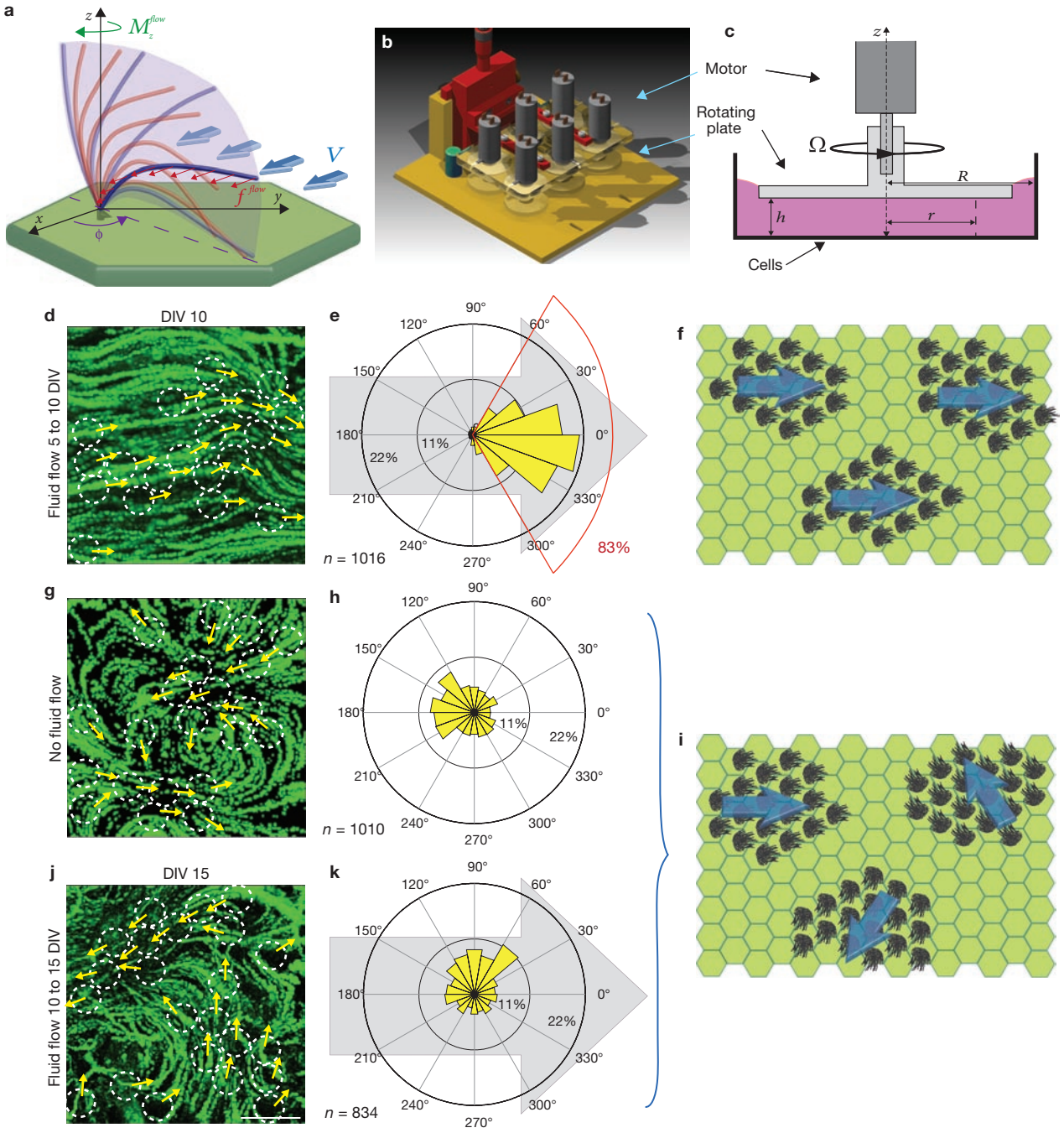

Figure 2 External fluid flow applied over ependymal cells during maturation orients subsequent ciliary beatings in its direction. (**a**) Schematic representation of a cilium beating with an angle $\phi \neq 0$ with the flow (V). Hydrodynamic forces (f^{flow}) act all over the cilium during its beating and create a torque (M_z^{flow}) that tends to rotate the cilium beating plane and its basal body and align it with the flow[9]. (**b**) Set-up made of 6 similar units used to apply a physiological-like shear flow over cultures (see Supplementary Information, Fig. S5). (**c**) Each motor rotates a circular plate dragging the medium in its rotation and creating a shear flow over cells. Both directions of rotation (clockwise and anticlockwise) were used equally in experiments. (**d**, **g**, **j**) Flow patterns generated by ciliary beatings in cultures where external flow was applied between 5–10 DIV (**d**), 10–15 DIV (**j**), and control cultures (**g**). In **g** and **j**, flow patterns are generated by two separate cell clusters. (**e**, **h**, **k**) Scoring of bead propelling directions in each condition and comparison with the applied local flow direction (grey arrow, Supplementary Information, Fig. S6). n is the number of analysed zones. (**f**, **i**) Schematic of three separate clusters of aligned multiciliated cells beating in a common (**f**) or independent directions (**i**). Scale bars, 5 cm (**b**) and 20 μm (**d**, **g**, **j**).

body appendices known to point in effective stroke direction[23] (Fig. 1c; Supplementary Information, Figs S2–S4). We compared the results with those obtained at a mature stage (P21, Fig. 1f). At P4, 53% of cells showed random circular distribution of basal bodies, compared with only 2% at P21 (according to Rayleigh's test for uniformity, cells called 'random cells' in the following; Fig. 1d, g, red arrows). Overall, ciliary alignment was significantly lower at P4, compared with P21, as shown by longer arrows ($<r_{Cell}>^{P4} = 0.56 \pm 0.05$ and $<r_{Cell}>^{P21} = 0.93 \pm 0.01$;

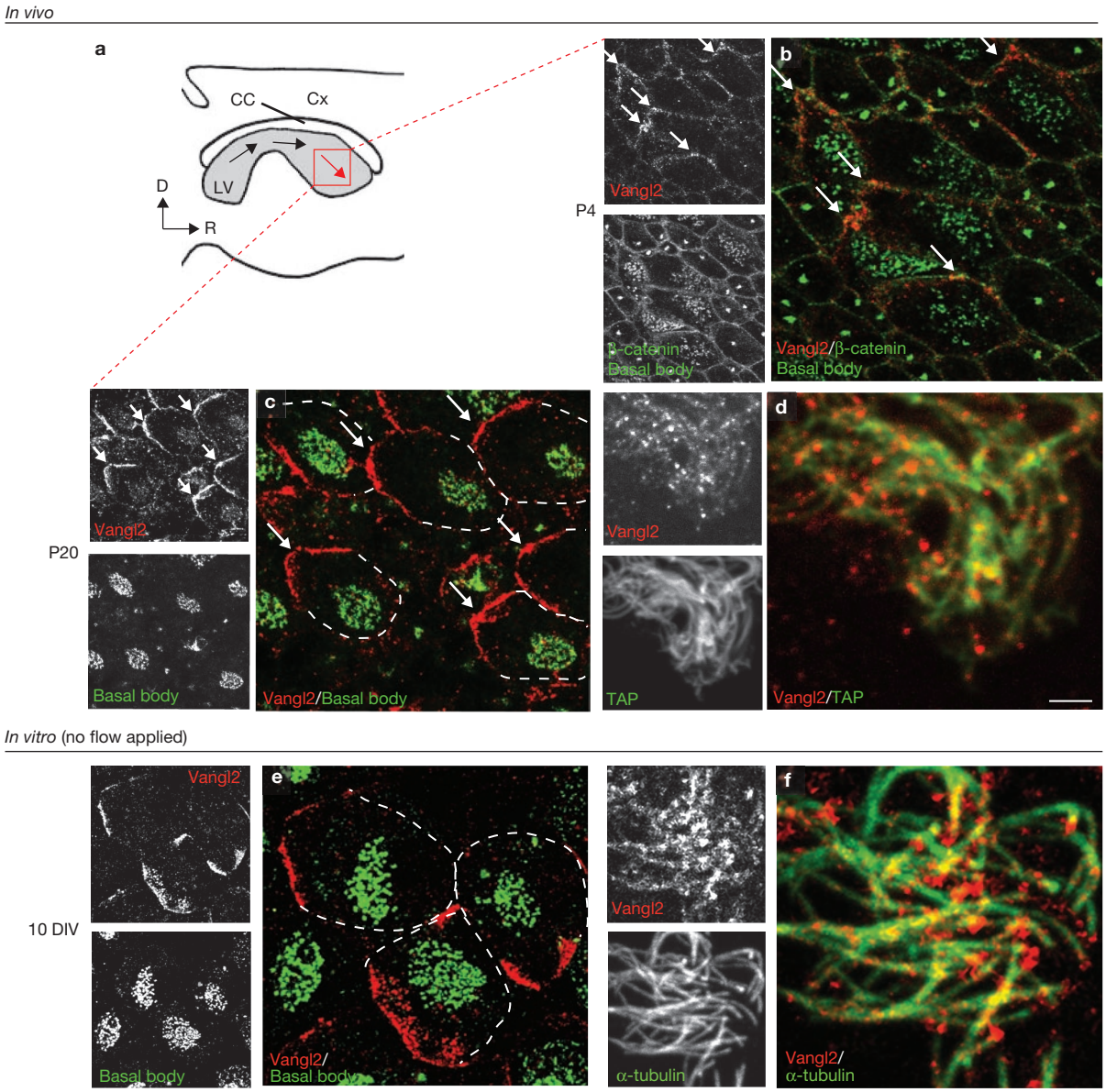

Figure 3 Vangl2 localizes asymmetrically at apical membrane and along cilia of multiciliated ependymal cells. (**a**) Schematic sagittal view of a mouse lateral ventricle wall. The red square indicates the region analysed in **b**–**d**. (**b**) Triple immunostaining with Vangl2 (red), β-catenin (cell borders, green) and CTR453 (basal bodies, green) antibodies at P4. (**c**) Double immunostaining with Vangl2 (red) and CTR453 (basal bodies, green) antibodies at P20 showing asymmetric localization of Vangl2 at the rear of multiciliated ependymal cells. (**d**) Double immunostaining with Vangl2 (red) and TAP (a cilia marker, green) antibodies showing ciliary localization of Vangl2 at P20 (see Supplementary Information, Movie 6). (**e**, **f**) Double immunostaining with Vangl2 (red) and CTR453 (green) or α-tubulin (cilia, green) *in vitro* at 10 DIV show asymmetric localization of Vangl2 at apical borders and along ependymal cilia *in vitro*. Scale bars, 5 μm (**b**, **c**), 3 μm (**e**) and 1.5 μm (**d**, **f**).

mean ± s.e.m, Fig. 1d, g; Supplementary Information, Fig. S4). Moreover, it is important to note that at P4, basal body alignment correlated with cell maturation: 100% of young cells (stage 2) were found to be random (Supplementary Information, Fig. S2g). Together, these observations show that basal bodies first dock at the cell membrane with random orientations spanning 360°, and progressively align in the direction of CSF flow during development.

To further study ciliary orientation in ependymal cells, we developed an *in vitro* culture assay of pure neural stem cells (NSC), isolated from neonatal mouse subventricular zone, that progressively differentiate into multiciliated ependymal cells. At 0 day *in vitro* (DIV), all cells were nestin-positive NSC[24] and by 15 DIV, up to 80 ± 6% became CD24-positive (a marker of ependymal cells[25]) multiciliated cells (Figs 1k, 4c, black curve). Most interestingly, by 10 DIV, 60% of cultured cells appeared in clusters of multiciliated cells surrounded by non-ciliated cells, suggesting that ependymal differentiation signal may be transduced through a cell–cell contact signalling pathway (Fig. 1l). At the cellular level, TEM analysis showed that 5 DIV cells shared similar immaturity features with *in vivo* P4 cells, such as electron dense aggregates[22] (red arrowhead in Fig. 1j; Supplementary Information, Fig. S2), and showed a smaller degree of alignment when compared with mature cells (>10 DIV; Figs 1j, m and 4f). We also used

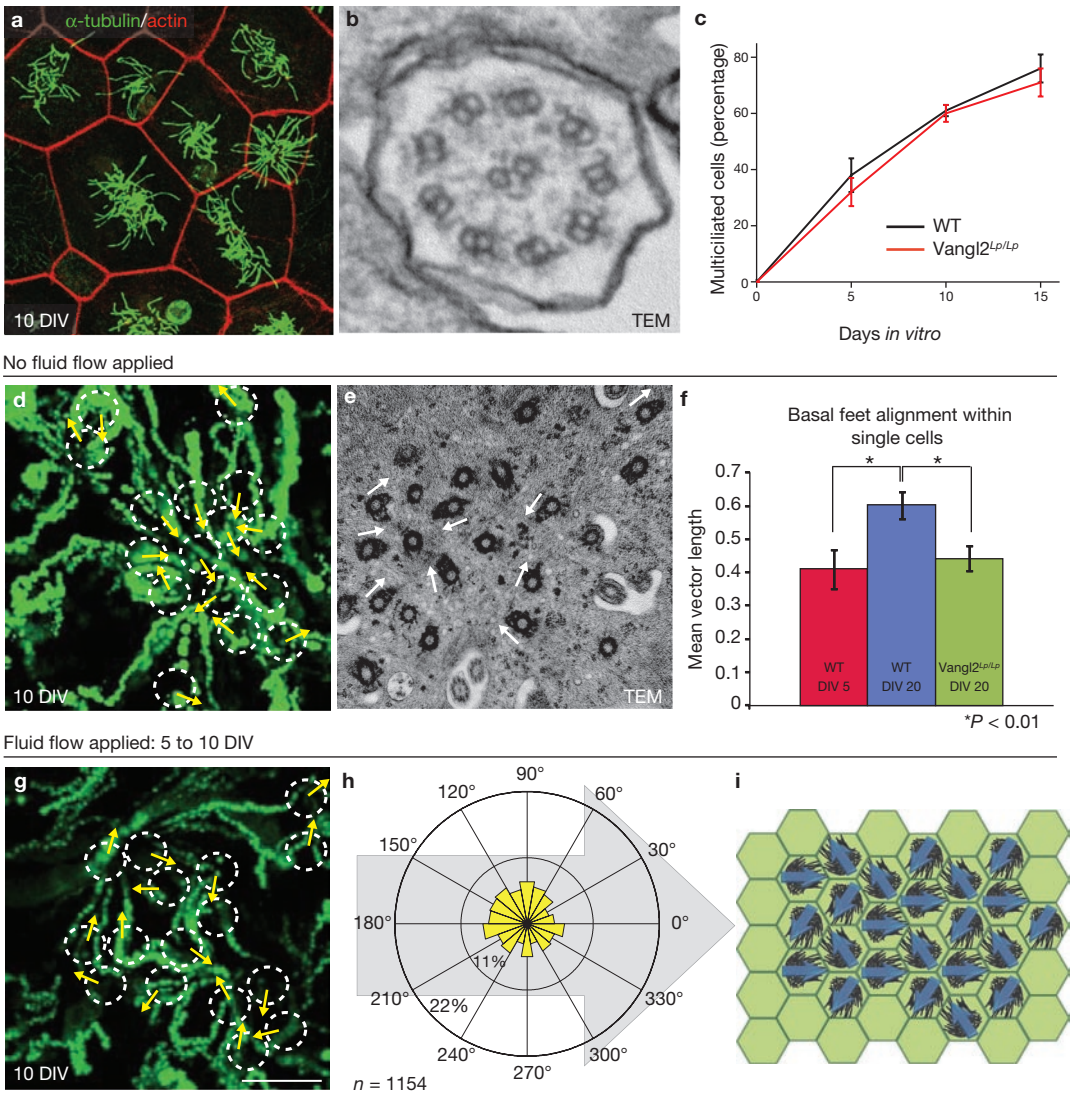

Figure 4 Vangl2 is required for cilia orientation response to flow *in vitro*. (**a**) Primary cultures of neural stem cells from Vangl2$^{Lp/Lp}$ E18.5 brains differentiate into multiciliated ependymal cells after 10 DIV. Cilia are stained with antibodies against detyrosinated α-tubulin (1D5, green) and cell borders are stained with phalloidin (actin, red). (**b**) TEM of a cilium transverse cut showing normal ciliary ultrastructure. (**c**) Increase in the percentage of multiciliated ependymal cells over time in wild-type (WT) and Vangl2$^{Lp/Lp}$ cultures. In both cultures, about 70% of neural stem cells differentiated into multiciliated ependymal cells by 15 DIV. (**d**, **g**) Bead trajectories in cultures from Vangl2$^{Lp/Lp}$ mutants without (**d**) or with (**g**) flow applied from 5–10 DIV. (**e**, **f**) TEM analysis and quantification of ciliary alignment in 15 cells (121 basal feet) from WT cultures at 5 DIV, 41 cells (352 basal feet) from WT cultures at 20 DIV and 32 cells (294 basal feet) from Vangl2$^{Lp/Lp}$ cultures at 20 DIV. Error bars represent s.d. (**h**) Quantitative analysis of propelling directions confirmed no correlation with external flow (*n* is the number of analysed zones). (**i**) Schematic representation of a cluster made of multiciliated cells beating in every direction. Scale bars, 20 μm (**a**), 0.1 μm (**b**), 20 μm (**d**, **g**) and 1 μm (**e**).

video microscopy and fluorescent beads to monitor cilia-generated flow in these cultures at different maturation times. Young cultures (~5 DIV) showed isolated multiciliated cells propelling beads slowly in random directions (Figs 1h, i; Supplementary Information, Movie 1), whereas older cultures (>10 DIV) had clusters of cells propelling beads faster in a common direction (Figs 1k, l and 2g, i; Supplementary Information, Movies 2–4). These observations show that single cells are able to progressively align their cilia. In addition, individual clusters of ciliated cells are able to align spontaneously their ciliary beating and propel fluid efficiently in one preferred direction. Global tissue polarization signals, as might be present *in vivo*, are not necessary for this process.

Hydrodynamic forces instruct ciliary beating orientation

Many studies have reported a correlation between impaired ciliary beating and disruption of basal body alignment[7,14,26,27], but mechanisms of ciliary orientation remain poorly understood. When the beating plane of a cilium is not aligned with the external flow, hydrodynamic forces acting all over the cilium during its beating tend to orient it in the direction of flow[9] (Fig. 2a). If its basal body can rotate within the cell cortex, the flow can reorient the cilium beating plane in its direction. Our theoretical study[9] showed that hydrodynamic interactions between cilia can lead to their spontaneous collective alignment in a positive-feedback mechanism, provided that their beat frequency or amplitude are large enough. This mechanism could explain the spontaneous alignment of

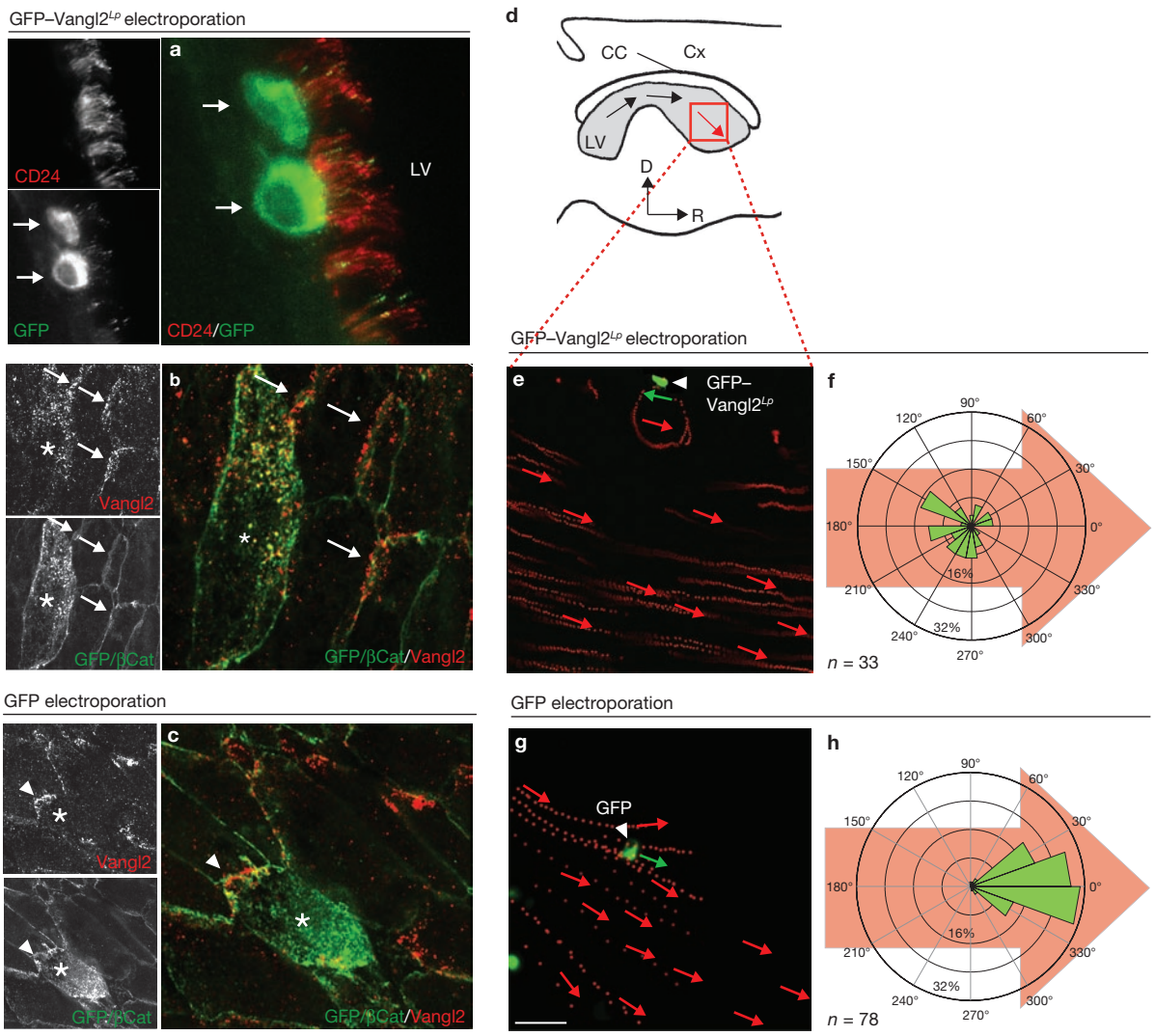

Figure 5 Vangl2 is required for *in vivo* cilia orientation. (**a**) At P20 (20 days post-electroporation), GFP–Vangl2^{Lp} electroporated cells were observed lining the lateral ventricular walls (GFP, green, white arrows; CD24, red). (**b**, **c**) Triple immunostaining of P20 lateral ventricular walls with Vangl2 (red), GFP (green) and β-catenin (green) antibodies. In GFP–Vangl2^{Lp} electroporated cells, Vangl2 accumulated in cytoplasm aggregates but failed to accumulate at the caudal membrane as compared with neighbouring cells (arrows) or cells electroporated with GFP alone (arrowhead in **c**). Stars indicate electroporated cells. (**d**) Schematic sagittal view of a mouse lateral ventricle wall. The red square indicates the ventricular wall region analysed in **e** and **g**. (CC, Corpus Callosum; Cx, cortex; LV, lateral ventricle; R, rostral; D, dorsal. (**e**, **g**) Bead trajectories at P20 show global caudo-rostral-directed flow corresponding to aligned ciliary beatings (red arrows), except in the vicinity of GFP–Vangl2^{Lp} electroporated cells (arrowhead in **e**), showing random beating orientations (green arrow; Supplementary Information, Movies 10–12). In contrast, GFP-electroporated cells (arrowhead in **g**) propel beads in the same direction as their neighbours (Supplementary Information, Movies 12–13). (**f**, **h**) Quantitative analysis showing random propelling directions of GFP–Vangl2^{Lp} electroporated cells (**f**) in contrast to GFP-electroporated cells, which propel beads in the caudo-rostral direction (**h**). Scale bars, 15 μm (**a**), 10 μm (**b**, **c**) and 100 μm (**e**, **g**).

ciliary beating at cluster level observed in our cultures (Supplementary Information, Fig. S1c–e) and the lack of alignment of impaired cilia described in previous studies[7,14,26,27].

To further address whether hydrodynamic forces may instruct ciliary beating orientation in mouse ependymal cells, we developed an experimental set-up to apply controlled shear flow over cell cultures during several days of growth (Fig. 2b, c; Supplementary Information, Fig. S5). This flow was approximately straight and uniform over each zone of analysis (Supplementary Information, Fig. S5e–f) and the shear stress τ was comparable to physiological values (see Methods). We applied continuous flow over maturing cell cultures at 5 DIV for 5 days, and analysed the direction of ciliary beating after the set-up was removed at 10 DIV. We scored fluorescent bead-propelling directions and compared them with the local direction of the applied flow (Supplementary Information, Figs S5e, S6). We found that cilia-propelling directions are significantly oriented towards the direction of the flow applied during growth (83% lie within a 120° angle window centred on the direction of external flow, which was set to 0°; Fig. 2d–f; Supplementary Information, Movie 3). Control cultures without flow showed typical cell clusters (Fig. 2g–i; Supplementary Information, Movie 4). This shows that hydrodynamic forces exerted on cilia during the ependymal cell maturation period drive their reorientation in the direction of flow. Interestingly, if the external flow was applied over more mature cells (between 10 and 15 DIV), no significant reorientation of ciliary beating directions was observed

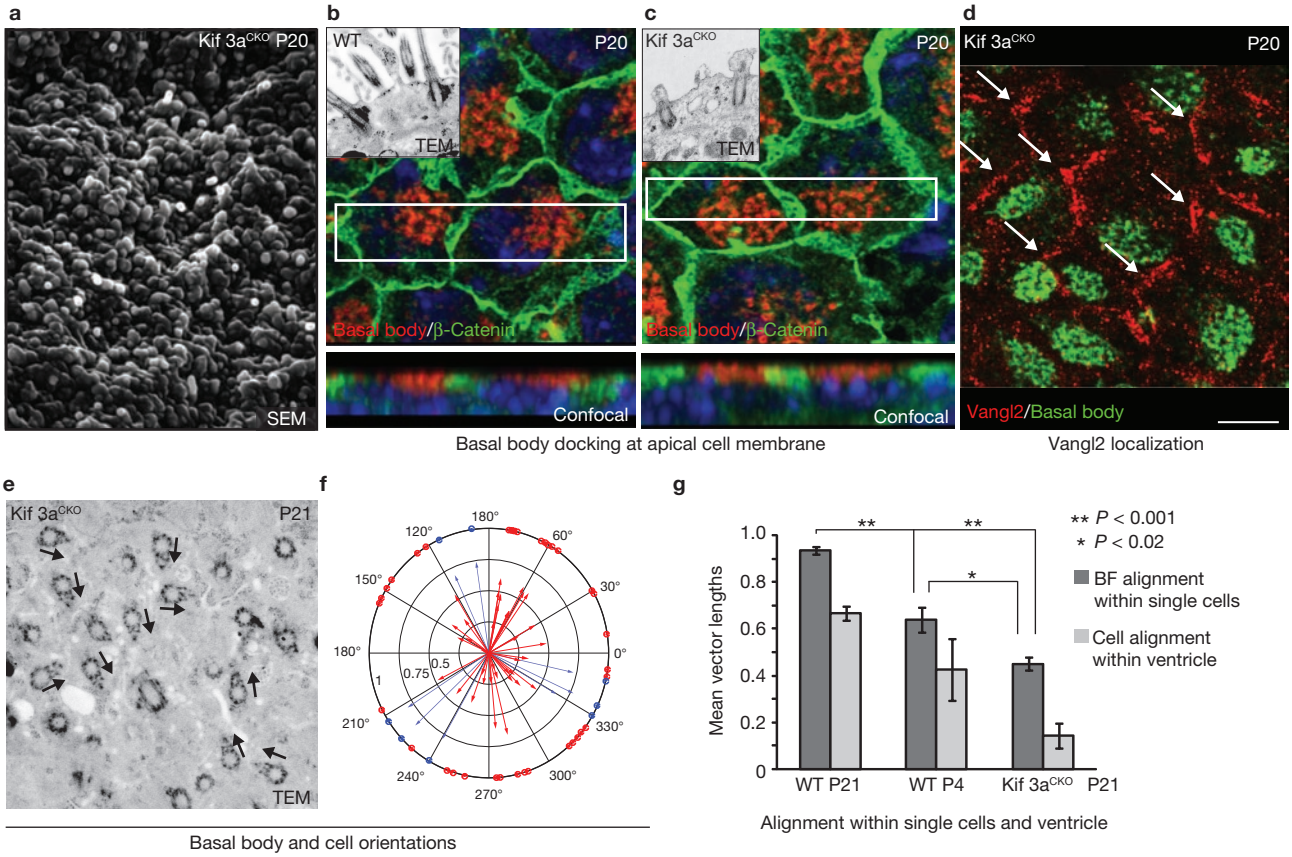

Figure 6 Kif3a^{CKO} ciliary mutant cells show proper apical asymmetric localization of Vangl2 but random orientation of basal bodies. (**a**) SEM of Kif3a^{CKO} lateral ventricular wall at P20. (**b**, **c**) Confocal and TEM images showing basal bodies (red) at the apical cell membrane in wild-type (**b**) and in Kif3a^{CKO} mutants (**c**); green: cell junctions (β-catenin), blue: nucleus (DAPI). (**d**) Vangl2 shows proper asymmetric localization at the rear of Kif3a^{CKO} mutant cells (white arrows). (**e**, **f**) TEM of Kif3a^{CKO} mutant cells showing impaired orientation of basal feet pointing in every direction (**e**) and quantification of basal feet orientation within 44 cells (433 basal bodies) in 2 mice (**f**). (**g**) Quantification of ciliary alignment at single cell level (dark grey) and cell alignment at ventricular level (light grey) in wild-type (WT) mice at P4 (30 cells, 305 basal bodies, Fig. 1 data set), P21 (49 cells, 563 basal bodies, Fig. 1 data set) and in Kif3a^{CKO} mice at P21 (44 cells, 433 basal bodies). BF, basal feet. Error bars represent s.d. Scale bars, 6 μm (**a**, **d**), 5 μm (**b**, **c**), 1.1 μm (**b** and **c** insets) and 0.7 μm (**e**).

(Fig. 2i–j; Supplementary Information, Movie 5), showing that cilia orientation in response to external flow is limited in time. These results thus reveal an orientation mechanism for motile cilia in mammals: ependymal cells in maturation orient their ciliary beating in response to hydrodynamic forces, and subsequently lock their ciliary orientation as they become mature.

Vangl2 localizes asymmetrically at the apical membrane and along cilia

To identify a molecular basis for this mechanism of ciliary orientation in response to flow, we tested the possible involvement of PCP signalling. We studied the expression pattern of the core PCP protein Van Gogh-like 2 (Vangl2)[18] during development in mouse lateral ventricles (Fig. 3a–d). At P4, all maturation stages of ependymal cells were present and Vangl2 protein was localized at the apicocaudal borders of nearly all cells with multiple basal bodies (Fig. 3b, arrows), suggesting that its asymmetric localization appears with ependymal cell differentiation. At P20, when most ependymal cells were mature, asymmetric accumulation of Vangl2 was stronger (arrows in Fig. 3c; Supplementary Information, Fig. S7a) and was undetectable in fully mature cells (>P45; data not shown). In addition, we found that Vangl2 also localized along cilia, from tip to base (Fig. 3d; Supplementary Information, Movie 6), presumably at the membrane, as it is a 4-pass transmembrane protein. *In vitro*, Vangl2 localization along ependymal cilia was also observed (Fig. 3f), as well as its spontaneous asymmetric localization at all stages analysed (stage 10 DIV shown in Fig. 3e and Supplementary Information, Fig. S7b; stages 5 and 15 DIV not shown), including after the locking of cilia orientation. Together, these results reveal a transient asymmetrical localization of a core PCP protein, Vangl2 during the whole ciliary orientation process of ependymal cells.

Vangl2 is required for ependymal cilia orientation in response to flow

To test whether Vangl2 is involved in ciliary orientation response to flow, we used *in vitro* cell cultures from Vangl2$^{Lp/Lp}$ mutants expressing the non functional *looptail* (*Lp*) form of Vangl2 (ref. 28). These cultures showed normal ciliogenesis, with normal axonemal ultrastructure and normal kinetics of development (Fig. 4a–c), suggesting that Vangl2 is neither required for ciliogenesis, nor for differentiation. Similarly to inner ear cells[26], Vangl2 staining showed that the Vangl2^{Lp} protein accumulates in aggregates in the cytoplasm but fails to accumulate at the cell membrane (Supplementary Information, Fig. S7c, d). Phase-contrast video microscopy analysis showed that the frequency and amplitude of ciliary beating in Vangl2$^{Lp/Lp}$ cultures are similar to wild-type cells (Supplementary Information, Movies 7, 8). However,

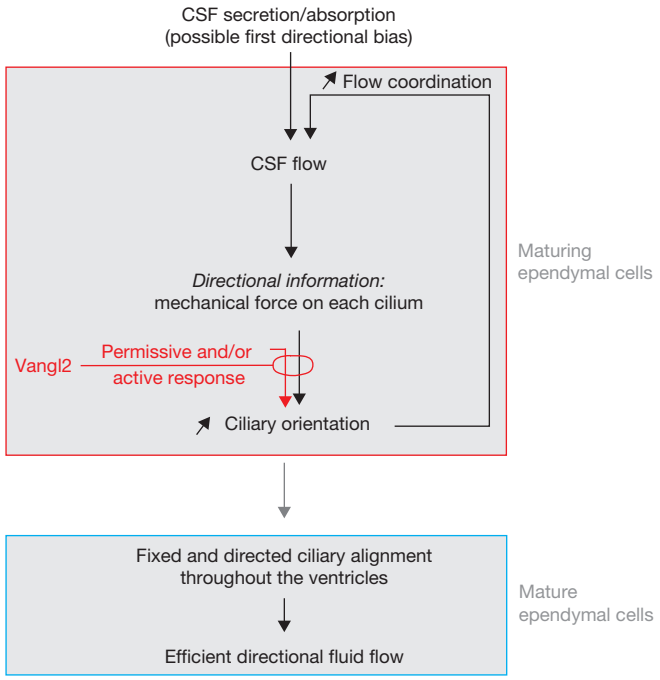

Figure 7 Motile cilia alignment reveals a new mechanism that couples hydrodynamic forces and PCP signalling. During the ependymal maturation period, because of secretion and absorption of CSF, flow is very likely to exist in the neural tube before motile cilia. As cilia form and start beating, hydrodynamic forces from the flow of CSF could orient their beating and align them along the direction of flow [9]. The flow of CSF could thus constitute an initial direction bias providing a long-range polarity signal during cilia growth, which tends to orient them along the caudo-rostral axis. As we have shown in this paper, the PCP core protein Vangl2 was found to localize at cilia and is required in the ciliary alignment response to flow. Vangl2 may either deliver a permissive response allowing the cilia (and their basal bodies) to rotate within the cell cortex under the influence of hydrodynamic forces, or be involved in an active response that would drive their reorientation, possibly by acting on the cytoskeleton surrounding basal bodies. As a result, ciliary alignment in the direction of flow increases and reinforces the CSF flow, following a positive-feedback loop, consistent with observations in *Xenopus* larvae[14]. Following this mechanism, by the end of maturation period, all cilia become aligned in the direction of flow. We show that this alignment mechanism is only active within a limited 'plastic' time-frame during maturation. Cilia orientation becomes permanently set in mature cells in which cilia no longer respond to flow. This plastic orientation mechanism would provide good adaptive features to surface irregularities and would ensure ciliary alignment at the tissue scale. Our work identifies a direct link between hydrodynamic cues and the PCP signalling pathway.

we discovered that in the Vangl2$^{Lp/Lp}$ cultures, ciliated cells propelled beads in random directions with many swirls in each cluster, in contrast to the wild-type cell clusters (Fig. 4d; Supplementary Information, Movie 9). Quantitative TEM analysis of basal feet orientation in culture showed that ciliary alignment in a given cell was significantly smaller in 20 DIV Vangl2$^{Lp/Lp}$ mutants, compared with 20 DIV wild-type cells (Fig. 4e, f): $<r_{Cell}>= 0.44 \pm 0.04$ and 72% of random cells for Vangl2$^{Lp/Lp}$, and $<r_{Cell}>= 0.6 \pm 0.04$ and 41% of random cells for wild-type cultures. Hence, neighbouring cilia do not influence each other at the cluster or cell level. Interestingly, these data show that Vangl2 is not required for proper ciliation and ciliary beating, but seems to be involved in ciliary orientation in response to hydrodynamic forces.

To further test this idea, we applied continuous fluid flow over maturing Vangl2$^{Lp/Lp}$ at 5 DIV cell cultures for 5 days, and analysed beating directions after removing the set-up at 10 DIV. Interestingly, Vangl2$^{Lp/Lp}$ cultures that were exposed to flow showed no preferential beating orientation, as shown by the quantitative analysis of bead trajectories, which did not correlate with the applied flow direction (Fig. 4g–i). These results show that Vangl2 is required for ciliary alignment response to flow during ependymal cell maturation.

Vangl2^{Lp} overexpression *in vivo* disturbs Vangl2 localization and ciliary beating orientation

Next, we investigated whether Vangl2 is also required for cilia orientation *in vivo*, where CSF circulates through the brain ventricles, using postnatal *in vivo* electroporation[29,30]. This method targets radial glia cells, precursors of ependymocytes, in the walls of P0 lateral ventricles[29,31].

Using this system we generated CD24-positive ependymocytes expressing a construct containing the coding sequence of the non-functional Vangl2^{Lp} protein[32] in fusion with GFP (GFP–Vangl2^{Lp}). The construct we used (see Methods) allowed strong and stable expression of GFP–Vangl2^{Lp} at 20 days post-electroporation (P20, Fig. 5a). In this situation, mislocalization of Vangl2 immunoreactivity was observed in 82% of GFP-positive ependymal cells (9/11 analysed cells from 3 mice). Indeed, Vangl2 accumulated in cytoplasm aggregates but failed to accumulate at the caudal membrane (Fig. 5b), consistent with the observations in cultures derived from Vangl2^{Lp} mice (Supplementary Information, Fig. S7c, d). By contrast, surrounding, non-transgenic cells (Fig. 5b, arrows) or cells expressing GFP only (Fig. 5c; 10/10 analysed cells from 3 mice) showed normal asymmetric distribution of Vangl2. These results show that expression of Vangl2^{Lp} is functionally dominant and disturbs the normal Vangl2 pathway, as suggested in previous studies[33,34].

Then, we analysed the directionality of ciliary beating of isolated transgenic cells expressing either GFP–Vangl2^{Lp} or GFP alone, by visualizing fluorescent bead trajectories on whole-mount preparations of lateral ventricles. GFP–Vangl2^{Lp}-expressing cells showed random propelling directions, in contrast to their GFP-negative neighbours, all of which propelled beads in a common caudo-rostral direction (Fig. 5e, f; Supplementary Information, Movies 10–12). Cells expressing only the GFP protein propelled the beads in the same direction as their GFP-negative neighbours (Fig. 5g, h; Supplementary Information, Movies 13, 14). Vangl2 is thus required for ependymal ciliary alignment response to flow *in vivo* in a cell autonomous manner. Together with the *in vitro* results, this shows that the mammalian ciliary orientation process couples hydronamic forces and the PCP protein Vangl2.

Ciliary mutant cells show proper Vangl2 asymmetric localization but randomized basal body orientation

To study cilia involvement and to further analyse how the core PCP protein Vangl2 is involved in ciliary alignment, we used a conditional mutant mouse deprived of ependymal cilia because of the absence of the protein Kif3a, which is involved in ciliogenesis (Kif3a^{CKO}, Fig. 6a)[35]. Basal bodies are normally docked at the apical membrane of Kif3a^{CKO} mutant cells and Vangl2 keeps its proper apicocaudal localization (Fig. 6b–d), showing that this asymmetry does not involve cilia-related information, and suggesting that Kif3a^{CKO} ventricles maintain normal polarization. However, at P21, basal feet were randomly oriented in Kif3a^{CKO} mutant cells ($<r_{Cell}>^{Kif3aCKO} = 0.45 \pm 0.03$; 80% random cells; Fig. 6e, f, g dark grey). At the tissue level, analysis of cell direction (arrows in polar diagrams) allows quantification of cell alignment

in ventricles (Supplementary Information, Fig. S4). Although wild-type ventricles showed increasing cell alignment during development ($<r_{Ventricle}>^{P4} = 0.42 \pm 0.13$; $<r_{Ventricle}>^{P21} = 0.67 \pm 0.03$), P21 Kif3a^{CKO} ventricles had cells pointing in random directions ($<r_{Ventricle}>^{Kif3aCKO} = 0.14 \pm 0.05$; Fig. 6g light grey), showing complete absence of cell alignment. We reproduced this experiment with the Ift88^{CKO} ciliary mutant[36] (Ift88 is also a protein required for ciliogenesis) and, similarly, we observed ependymal cells with disorganized basal body orientation, despite proper Vangl2 apicocaudal localization (Supplementary Information, Fig. S8a–c). This confirms the involvement of cilia rather than Kif3a in the orientation process. Interestingly, our results show that the asymmetric localization of Vangl2 is not sufficient to orient, or even bias, basal bodies at the tissue and cell levels, as could have been suggested by a previous study[17]. Together with the random orientation of basal bodies found in young ependymal cells (Fig. 1; Supplementary Information, Fig. S2), this shows the absence of a cilia-independent pre-patterning that would bias basal body docking orientation in the ventricular walls, as opposed to what was described in *Xenopus*[14,17].

DISCUSSION

Our results support an original orientation mechanism for ependymal cilia, whereby basal bodies first dock apically with random orientations, and then reorient in a common direction in response to coupling between hydrodynamic forces and the PCP pathway, within a definite time-frame (Fig. 7). Interestingly, we have shown that none of these signals can act on its own, as could have been hypothesized on the basis of other studies[9,16–18].

Such a mechanism is different from the two-step process described in *Xenopus* larvae skin. There, outer non-ciliated epithelial cells instruct the orientation of intercalating ciliated cells through a non-cell autonomous PCP pathway, biasing the orientation of basal bodies docking along the embryonic axis, independently of ciliary function. This bias enables the creation of a directed fluid flow that allows subsequent refinement of ciliary alignment[14,17]. Instead, in the brain ventricles, we found no bias in the orientation of basal body docking, either in young wild-type cells (Fig. 1c, d, S2g) or in mature cells from our ciliary mutants (Fig. 6e–g; Supplementary Information, Fig. S8a–c), indicating the absence of pre-patterning in basal body docking. Moreover, our *in vivo* Vangl2^{Lp} electroporation experiments argue in favour of a cell-autonomous polarization of basal bodies, as isolated electroporated cells beat in random orientation and were not rescued by their non-electroporated neighbours (Fig. 5e, f; Supplementary Information, Movies 10–12). Thus, the CSF flow would provide the initial long-range polarization bias leading to ciliary alignment at the tissue level. Indeed, in mammalian lateral ventricles, a pressure gradient arising from CSF secretion in the choroid plexus (developing from embryonic day 14) and absorption in the foramen of Monroe is very likely to initiate CSF flow in the caudo-rostral direction before cilia growth[37,38]. Hydrodynamic forces would thus align young randomly oriented cilia in the direction of flow when they start beating, enhancing CSF flow by a positive-feedback mechanism[9,14] (Fig. 7).

The major feature of the mechanism highlighted here is the interplay between hydrodynamic forces and a PCP pathway mediated by Vangl2. How might this coupling be achieved? The requirement of cilia in basal body polarization, and the localization of Vangl2 along them, suggest that this coupling could involve ciliary Vangl2. Located from cilium tip to base, Vangl2 lies in a central position between 'sensor' proteins such as polycystins, mutants of which develop hydrocephalus[39], and basal body localized Vangl2 effectors such as Dishevelled[40], which is involved in *Xenopus* basal body pre-patterning[16], and that localizes at ependymal basal bodies (Supplementary Information, Fig. S8d, e). Vangl2 could therefore be involved in a sensing signalling pathway that could either lead to a permissive response where cilia would rotate in the cell cortex under the influence of hydrodynamic forces and align with the flow, and/or a more active response that would polarize the cytoskeleton and reorient basal bodies in the flow direction. The genetic interaction between Bardet Biedl Syndrome (BBS) proteins and Vangl2, reported in mouse cochlea, is consistent with this second hypothesis[41,42]. Given the spotty Vangl2 staining that resembles that of intraflagellar transport proteins (IFT)[43], and the fact that BBS4 is present in the cochlear cell cilium[44] and was shown to be involved in the targeting of cargos toward the pericentriolar region[45], it would be interesting to test whether 'activation' of Vangl2 in response to flow could be its loading on IFTs and targeting to the basis of the cilium[46–48], where it could interact with Dishevelled localized in the vicinity of basal bodies. Vangl2 was previously described along human respiratory cilia, which were recently found to have sensory functions[49], suggesting that similar mechanisms may exist in other organs[41]. Ependymal cilia also express receptors for EGF[50], PDGFA[50] and P2X7 (ref. 51): this argues for their sensory function and is consistent with the major role of ependymal cells in neuroblast migration[8], and as primary cells generating neurons and glial cells after stroke[52].

This ciliary alignment mechanism uncovers a direct link between fluid-mediated orientation and the PCP pathway, adding hydrodynamic forces to the signalling cues influencing PCP. According to this mechanism, the CSF flow could constitute the initial polarization cue that biases ciliary orientation, replacing the pre-patterning observed in other epithelia[17,19]. It also provides a long-range polarity signal that extends beyond cell neighbours, adapts to surface irregularities and ensures ciliary polarization throughout the tissue. In addition, this coupling provides flow-induced ciliary orientation with a pathway specialized in cytoskeleton asymmetric reorganization. The molecular deciphering of this coupling, which could be relevant in polarization of other type of mammalian cilia, is of prime interest to better understand ciliary dysfunctions involved in human diseases and to study morphogenesis mediated by fluid flow[53]. □

METHODS

Methods and any associated references are available in the online version of the paper at http://www.nature.com/naturecellbiology/

Note: Supplementary Information is available on the Nature Cell Biology website.

ACKNOWLEDGMENTS

We thank A. Buguin, B. Lemaire and J.-H. Codarbox for their help with the flow set-up realization. We thank Marie-Paule Muriel for excellent technical assistance and for having shared her T.E.M. background. We thank the Pitié-Salpêtrière and Cochin hospitals imaging centres. We thank B. Yoder (University of Alabama, Birmingham) and L.S. Goldstein (University of California San Diego) for providing us with *Ift88*$^{fl/fl}$ and *Kif3a*$^{fl/KO}$ mice, respectively. We thank A. Alvarez-Buylla for making *Ift88*$^{fl/fl}$ mice available. We thank M. Bornens for the gift of CTR453 antibody, X. Morin for the gift of pCX plasmid and MH. Bré for the gift of TAP antibody. We also thank M. Bornens, B. Durand, J.-F. Joanny and Y. Bellaïche for discussions and reading of this manuscript. This work was supported by grants from the Agence Nationale de la Recherche (to N.S.), The International Human Frontier Science Program Organization (to N.S. and K.S.), the Fondation NRJ-Institut de France (to N.S.), the Mairie de Paris start-up Grant (to N.S.), by Fondation pour la Recherche Médicale and AXA Research Funds fellowships to A.M. and Neuropole de Recherche Francilien fellowship to J.-M.C. B.G. and A.A. were fellows of the Ministère de l'enseignement supérieur et de la recherche.

AUTHOR CONTRIBUTIONS

A.M. designed the study, performed and analysed experiments; B.G. designed the flow set-up, designed, performed flow experiments, and analysed experiments; S.M. performed and analysed videomicroscopy experiments; L.S. performed multiciliated ependymal cell cultures; A.A. and J.-M.C. performed *in vitro* experiments; A.D. and C.B. performed electroporation experiments; H.C. supervised the electroporation experiments; M.M. made the Vangl2$^{Lp/Lp}$ mice available, provided Vangl2^{Lp} construct and Vangl2 antibody, and contributed to many discussions; Y.H. performed India ink experiments; Y.-G.H. provided conditional Ift88 mice; Z.M. prepared conditional Ift88 samples; K.S. designed the study and supervised India ink experiments; N.S. initiated the study, designed, performed and analysed experiments, and supervised the project; N.S., A.M. and B.G. wrote the manuscript. All authors commented on the manuscript.

COMPETING FINANCIAL INTERESTS.

The authors declare no competing financial interests.

Published online at http://www.nature.com/naturecellbiology/
Reprints and permissions information is available online at http://npg.nature.com/reprintsandpermissions/

1. Machemer, H. Ciliary activity and the origin of metachrony in Paramecium: effects of increased viscosity. *J. Exp. Biol.* **57,** 239–259 (1972).
2. Hirokawa, N., Tanaka, Y., Okada, Y. & Takeda, S. Nodal flow and the generation of left-right asymmetry. *Cell* **125,** 33–45 (2006).
3. Ibanez-Tallon, I., Heintz, N. & Omran, H. To beat or not to beat: roles of cilia in development and disease. *Hum. Mol. Genet.* **12 Spec No 1,** R27–R35 (2003).
4. Banizs, B. *et al.* Dysfunctional cilia lead to altered ependyma and choroid plexus function, and result in the formation of hydrocephalus. *Development* **132,** 5329–5339 (2005).
5. Paltieli, Y. *et al.* High progesterone levels and ciliary dysfunction — a possible cause of ectopic pregnancy. *J. Assist. Reprod. Genet.* **17,** 103–106 (2000).
6. Ibanez-Tallon, I. *et al.* Dysfunction of axonemal dynein heavy chain Mdnah5 inhibits ependymal flow and reveals a novel mechanism for hydrocephalus formation. *Hum. Mol. Genet.* **13,** 2133–2141 (2004).
7. Lechtreck, K. F., Delmotte, P., Robinson, M. L., Sanderson, M. J. & Witman, G. B. Mutations in Hydin impair ciliary motility in mice. *J. Cell Biol.* **180,** 633–643 (2008).
8. Sawamoto, K. *et al.* New neurons follow the flow of cerebrospinal fluid in the adult brain. *Science* **311,** 629–632 (2006).
9. Guirao, B. & Joanny, J. F. Spontaneous creation of macroscopic flow and metachronal waves in an array of cilia. *Biophys. J.* **92,** 1900–1917 (2007).
10. Marshall, W. F. & Kintner, C. Cilia orientation and the fluid mechanics of development. *Curr. Opin. Cell Biol.* **20,** 48–52 (2008).
11. Tamm, S. L., Sonneborn, T. M. & Dippell, R. V. The role of cortical orientation in the control of the direction of ciliary beat in Paramecium. *J. Cell Biol.* **64,** 98–112 (1975).
12. Iftode, F. & Fleury-Aubusson, A. Structural inheritance in Paramecium: ultrastructural evidence for basal body and associated rootlets polarity transmission through binary fission. *Biol. Cell* **95,** 39–51 (2003).
13. Boisvieux-Ulrich, E., Sandoz, D. & Allart, J.-P. Determination of ciliary polarity precedes differentiation in the epithelial cells of quail oviduct. *Biol. Cell* **72,** 3–14 (1991).
14. Mitchell, B., Jacobs, R., Li, J., Chien, S. & Kintner, C. A positive feedback mechanism governs the polarity and motion of motile cilia. *Nature* **447,** 97–101 (2007).
15. Klein, T. J. & Mlodzik, M. Planar cell polarization: an emerging model points in the right direction. *Annu. Rev. Cell Dev. Biol.* **21,** 155–176 (2005).
16. Park, T. J., Mitchell, B. J., Abitua, P. B., Kintner, C. & Wallingford, J. B. Dishevelled controls apical docking and planar polarization of basal bodies in ciliated epithelial cells. *Nature Genet.* **40,** 871–879 (2008).
17. Mitchell, B. *et al.* The PCP pathway instructs the planar orientation of ciliated cells in the *Xenopus* larval skin. *Curr. Biol.* **19,** 924–929 (2009).
18. Montcouquiol, M. *et al.* Identification of Vangl2 and Scrb1 as planar polarity genes in mammals. *Nature* **423,** 173–177 (2003).
19. Devenport, D. & Fuchs, E. Planar polarization in embryonic epidermis orchestrates global asymmetric morphogenesis of hair follicles. *Nature Cell Biol.* **10,** 1257–1268 (2008).
20. Wang, Y. & Nathans, J. Tissue/planar cell polarity in vertebrates: new insights and new questions. *Development* **134,** 647–658 (2007).
21. Wu, J. & Mlodzik, M. A quest for the mechanism regulating global planar cell polarity of tissues. *Trends Cell Biol.* **19,** 295–305 (2009).
22. Spassky, N. *et al.* Adult ependymal cells are postmitotic and are derived from radial glial cells during embryogenesis. *J Neurosci* **25,** 10–18 (2005).
23. Frisch, D. & Farbman, A. I. Development of order during ciliogenesis. *Anat. Rec.* **162,** 221–232 (1968).
24. El Zein, L. *et al.* RFX3 governs growth and beating efficiency of motile cilia in mouse and controls the expression of genes involved in human ciliopathies. *J. Cell Sci.* **122,** 3180–3189 (2009).
25. Calaora, V., Chazal, G., Nielsen, P. J., Rougon, G. & Moreau, H. mCD24 expression in the developing mouse brain and in zones of secondary neurogenesis in the adult. *Neuroscience* **73,** 581–594 (1996).
26. Afzelius, B. A. The immotile-cilia syndrome and other ciliary diseases. *Int. Rev. Exp. Pathol.* **19,** 1–43 (1979).
27. Rautiainen, M., Collan, Y., Nuutinen, J. & Afzelius, B. A. Ciliary orientation in the "immotile cilia" syndrome. *Eur. Arch. Otorhinolaryngol.* **247,** 100–103 (1990).
28. Torban, E. *et al.* Tissue, cellular and sub-cellular localization of the Vangl2 protein during embryonic development: effect of the Lp mutation. *Gene Expr. Patterns* **7,** 346–354 (2007).
29. Boutin, C., Diestel, S., Desoeuvre, A., Tiveron, M. C. & Cremer, H. Efficient *in vivo* electroporation of the postnatal rodent forebrain. *PLoS ONE* **3**, e1883 (2008).
30. Boutin, C., Schmitz, B., Cremer, H. & Diestel, S. NCAM expression induces neurogenesis *in vivo*. *Eur. J. Neurosci.* **30,** 1209–1218 (2009).
31. Merkle, F. T., Tramontin, A. D., Garcia-Verdugo, J. M. & Alvarez-Buylla, A. Radial glia give rise to adult neural stem cells in the subventricular zone. *Proc. Natl Acad. Sci. USA* **101,** 17528–17532 (2004).
32. Montcouquiol, M. *et al.* Asymmetric localization of Vangl2 and Fz3 indicate novel mechanisms for planar cell polarity in mammals. *J. Neurosci.* **26,** 5265–5275 (2006).
33. van Abeelen, J. H. & Raven, S. M. Enlarged ventricles in the cerebrum of loop-tail mice. *Experientia* **24,** 191–192 (1968).
34. Vandenberg, A. L. & Sassoon, D. A. Non-canonical Wnt signaling regulates cell polarity in female reproductive tract development via van gogh-like 2. *Development* **136,** 1559–1570 (2009).
35. Spassky, N. *et al.* Primary cilia are required for cerebellar development and Shh-dependent expansion of progenitor pool. *Dev. Biol.* **317,** 246–259 (2008).
36. Haycraft, C. J. *et al.* Intraflagellar transport is essential for endochondral bone formation. *Development* **134,** 307–316 (2007).
37. Redzic, Z. B., Preston, J. E., Duncan, J. A., Chodobski, A. & Szmydynger-Chodobska, J. The choroid plexus-cerebrospinal fluid system: from development to aging. *Curr. Top. Dev. Biol.* **71,** 1–52 (2005).
38. Miyan, J. A., Nabiyouni, M. & Zendah, M. Development of the brain: a vital role for cerebrospinal fluid. *Can. J. Physiol. Pharmacol.* **81,** 317–328 (2003).
39. Wodarczyk, C. *et al.* A novel mouse model reveals that polycystin-1 deficiency in ependyma and choroid plexus results in dysfunctional cilia and hydrocephalus. *PLoS One* **4**, e7137 (2009).
40. Torban, E., Wang, H. J., Groulx, N. & Gros, P. Independent mutations in mouse Vangl2 that cause neural tube defects in looptail mice impair interaction with members of the Dishevelled family. *J. Biol. Chem.* **279,** 52703–52713 (2004).
41. Ross, A. J. *et al.* Disruption of Bardet-Biedl syndrome ciliary proteins perturbs planar cell polarity in vertebrates. *Nature Genet.* **37,** 1135–1140 (2005).
42. Jones, C. *et al.* Ciliary proteins link basal body polarization to planar cell polarity regulation. *Nature Genet.* **40,** 69–77 (2008).
43. Pazour, G. J., Wilkerson, C. G. & Witman, G. B. A dynein light chain is essential for the retrograde particle movement of intraflagellar transport (IFT). *J. Cell Biol.* **141,** 979–992 (1998).
44. May-Simera, H. L. *et al.* Patterns of expression of Bardet-Biedl syndrome proteins in the mammalian cochlea suggest noncentrosomal functions. *J. Comp. Neurol.* **514,** 174–188 (2009).
45. Kim, J. C. *et al.* The Bardet-Biedl protein BBS4 targets cargo to the pericentriolar region and is required for microtubule anchoring and cell cycle progression. *Nature Genet.* **36,** 462–470 (2004).
46. Qin, H. *et al.* Intraflagellar transport is required for the vectorial movement of TRPV channels in the ciliary membrane. *Curr. Biol.* **15,** 1695–1699 (2005).
47. Wang, Q., Pan, J. & Snell, W. J. Intraflagellar transport particles participate directly in cilium-generated signaling in *Chlamydomonas*. *Cell* **125,** 549–562 (2006).
48. Lechtreck, K. F. *et al.* The *Chlamydomonas reinhardtii* BBSome is an IFT cargo required for export of specific signaling proteins from flagella. *J. Cell Biol.* **187,** 1117–1132 (2009).
49. Shah, A. S., Ben-Shahar, Y., Moninger, T. O., Kline, J. N. & Welsh, M. J. Motile cilia of human airway epithelia are chemosensory. *Science* **325**, 1131–1134 (2009).
50. Danilov, A. I. *et al.* Ultrastructural and antigenic properties of neural stem cells and their progeny in adult rat subventricular zone. *Glia* **57,** 136–152 (2009).
51. Genzen, J. R., Platel, J. C., Rubio, M. E. & Bordey, A. Ependymal cells along the lateral ventricle express functional P2X(7) receptors. *Purinergic Signal.* **5**, 299–307 (2009).
52. Carlen, M. *et al.* Forebrain ependymal cells are Notch-dependent and generate neuroblasts and astrocytes after stroke. *Nature Neurosci.* **12,** 259–267 (2009).
53. Cartwright, J. H., Piro, O. & Tuval, I. Fluid dynamics in developmental biology: moving fluids that shape ontogeny. *HFSP J.* **3,** 77–93 (2009).

METHODS

Transgenic mice. All animal care was in accordance with the guidelines of the National Institutes of Health and European law. The Vangl2$^{Lp/Lp}$ mutant mice bearing the *Lp* mutation of *Vangl2* gene were described previously[18,28]. The *hGFAP-Cre* mouse line containing 2.2 kb of the hGFAP promoter linked to the coding region of Cre recombinase, *Kif3a*^{fl} mice containing loxP sites flanking exon 2 of the *Kif3a* gene, *Kif3a*$^{-/+}$ mice and *Ift88*$^{fl/fl}$ mice were described previously[35,36,54,55].

Electroporation. Plasmid: we used a Vangl2 fluorescent construct containing the *Lp* mutation. GFP–Vangl2^{Lp} expression cassette from the pGFP-C3–Vangl2^{Lp32} was inserted into a eukaryotic expression vector based on the chicken β-actin promoter and the CMV enhancer (pCX-MCS2, a derivative of pCAAGS[56]) to increase gene expression. Plasmids were prepared by using an EndoFree Plasmid Kit (Quiagen Maxiprep Kit, cat. no. 12362) and resuspended in PBS (final concentration 5 μg μl^{-1}).

Postnatal electroporation protocol: electroporations were performed as described previously[29]. Ciliary beating of GFP–Vangl2^{Lp} electroporated ependymal cells (GFP^{+}) were analysed by visualization of red fluorescent beads trajectories on whole-mount preparation immediately after dissection between P14 and P20.

Cultures. Cells from the subventricular zone of newborn mice were dissociated, resuspended in fresh medium, plated at high density in 10% FCS containing medium, and allowed to grow to confluence. Pure confluent astroglial monolayers were plated at a density of 7×10^4 cells/cm^2 and maintained in serum-free medium for ependymal differentiation.

Flow set-up. Rotating units and shear stress: each unit is made of one circular rotating plate in Plexiglas (3.2 cm diameter, manufactured at The Curie Institute, Paris, France), which is fixed to a motor rotating continuously (1271 series, gear ratio 188:1, 12V dc, McLennan). Each rotating plate is in contact with the culture medium in each well and drags it in its rotation thus creating a shear flow over cells. With such a set up, the shear stress τ applied upon cells depends on the circular plate rotation speed Ω, the distance from the axis r and the height of the plate h (Fig. 2b and Supplementary Information, Fig. S5d) and is given by: $\tau = \eta\,\Omega\,r/h$, η being the medium viscosity. All units are held together by a 6-hole Plexiglas plate which is fixed to a micrometric displacement set up that allows to settle precisely the height at which circular plates rotate, and therefore the shear stress applied. Everything is fixed on a duraluminium plate and connected to a power supply (Supplementary Information, Fig. S5c). It is worth noting that ciliated cell cultures did not differentiate in 'classic' flow chambers.

Power supply (Supplementary Information, Fig. S5c, inset) was designed and manufactured in The Curie Institute (Paris, France). It is connected to the set-up described above and converts the 220V AC from the mains into 15V DC and delivers a maximal intensity of 1A. Six sources of controlled tension are in parallel on this 15V generator providing each motor with power independently. Each source contains a potentiometer to adjust the tension at each motor between 2V and 12V, allowing tuning of each motor rotation speed and thus controlling the shear stress generated by each rotating plate in each culture.

We chose the parameters of the experimental study so that the shear stress applied during growth at distance r = 1 cm from the rotation axis, where culture will be subsequently analysed (Supplementary Information, Fig. S5e), remains comparable to physiological values for mature cells. We estimated the physiological shear stress τ_φ that cells experience *in vivo* by measuring bead mean velocity V above mature lateral ventricle walls (>P20), estimating the height h at which measurements were made. τ_φ is then given by $\tau_\varphi \approx \eta\,V/h$, ($\eta \approx 8\ 10^{-4}$ Pa.s for DMEM at 37°C[57]). We found $V \approx 45.6 \pm 2.5$ μm s^{-1} (n = 83 beads) measured at $h \approx 20$ μm leading to $\tau_\varphi \approx 1.8\ 10^{-3}$ Pa = 0.018 dyn/cm^2. Therefore, we applied a range of shear stress τ =1.0-1.8 10^{-3} Pa over cells in cultures. We generated this range of shear stress by setting the rotating plates at height h = 4 mm and by settling the rotation speed Ω in the range Ω = 5–8.6 rounds min^{-1}. Both directions of rotation (clockwise and anticlockwise) were equally used in our experiments.

Immunostaining. Brain ventricles and cell cultures were fixed in 4% paraformaldehyde (for F-actin, acetylated α-tubulin and CD24) or in methanol at –20°C (for β-catenin, CTR453, Vangl2, TAP, γ-tubulin, ZO1, Dvl1, GFP and acetylated α-tubulin). Tissues and cells were pre-blocked in PBS with 0.1% Triton X-100 and 10% fetal calf serum (FCS) and incubated overnight with the primary antibodies. The following antibodies were used: mouse IgG1 anti-β-catenin (1:500; Chemicon), mouse IgG2b anti-CTR453 (1:10; ref. 58), rabbit pAb anti-Vangl2 (1:500; ref. 32), mouse IgG1 anti-acetylated α-tubulin (1:1000, Synaptic Systems), rat anti-CD24 (1:100; BD Pharmingen), rabbit pAb anti-γ-tubulin (1:500, Sigma), rabbit pAb anti-dvl1 (1:200, Santa Cruz), rabbit pAb anti-GFP (1:200, Molecular Probes), rabbit anti-ZO1 (1:100, Zymed), rhodamin and fluorescein phalloidin anti-F-actin (1:1000; Invitrogen) and species-specific secondary antibodies (Molecular Probes or Jackson ImmunoResearch). Tissues and cells were counterstained with DAPI (10 μg ml^{-1}, Sigma), mounted in Fluoromount and examined with a fluorescent upright microscope or a fluorescent confocal microscope (DM IRBE and SP2 Leica). For acetylated α-tubulin and TAP immunostainings under methanol fixation, samples were pretreated with 0.1% Triton X-100 in PBS for 5 min before fixation to preserve cilia structure. For CD24 immunostaining, no Triton was used.

Microscopy. For scanning electron microscopy, brains ventricles were dissected as described previously[59] and viewed using a JEOL (Akishima, Japan) scanning electron microscope. For transmission electron microscopy, brains from P4 and P21 mice were sectioned into 200 μm slices using a vibratome (VT 1200S, Leica). Sections of the rostral lateral and dorsal walls of the lateral ventricle were taken apart in PBS under a dissecting microscope. Cultured cells or ventricle slices were fixed in 2.5% glutaraldehyde and 4% paraformaldehyde. Tissues were treated with 1% OsO4. Fixed specimens were washed and progressively dehydrated. Samples were then incubated in 1% uranyl acetate in 70% methanol. Final dehydratations were made. Samples were pre-impregnated with ethanol/epon mix (2/1, 1/1, 1/2 ratios subsequently), and impregnated into epon. Samples were then mounted into epon blocks for 48 h at 60°C to ensure polymerization. Ultrathin sections of 70 nm were cut using an ultramicrotome (Ultracut E, Reichert-Jung) and analysed using a Jeol 10-11 transmission electron microscope.

In vitro phase-contrast and fluorescent videomicroscopy were performed on a Zeiss inverted microscope (Axiovert 200M) fitted for immunofluorescence in a room with the temperature controlled at 27°C. Images were acquired with a CCD camera (ORCA-ER, Hammamatsu) operating in streaming mode. Time-lapse sequences were acquired to analyse 0.75 μm diameter fluorescent bead movements (fluoresbrite carboxylate microspheres, Polyscience). Time between two frames was 1 s; exposure time was 470 ms per frame; binning was 2 × 2 pixels. *Z* projection of the maximum intensity of a stack of 100 slices represent beads trajectory. *In vivo* videomicroscopy was performed on a Leica DM IRB inverted microscope. Time-lapse sequences were acquired with a CCD camera (C4742-95, Hammamatsu) using OpenLab™ software. Time between two frames was 273 ms; exposure time was 11 ms per frame; binning was 1 × 1 pixels.

Data analysis. For analysis of basal body orientation: basal bodies scoring, measurement of mean polar orientation of ciliated cells and average circular standard deviation (CSD) calculation is described in Supplementary Information, Fig. S4. Circular data were plotted on circular diagram: arrow angle (α_{Cell}) represents the mean ciliary direction of cells and arrow length (r_{Cell}) represents 1-circular variance of cilia within the cell. Circular distribution of basal bodies in each cell was compared to a uniform distribution using the Rayleigh test (P <0.05). Values for vector lengths were compared using a two-tailed unpaired Student's t-test when distributions were found to be normal, otherwise two-tailed Mann-Whitney test was used. Circular and linear statistics were done with StatistXL software (Broadway). Circular plots were done with Matlab (The Mathworks). All averaged data are given as mean ± s.e.m.

For analysis of bead-propelling directions, fluorescent video-microscopy images were first reoriented according to their location in the culture so that the applied flow direction always points horizontally toward the right. From the stacks of images, two-dimensional bead trajectories were obtained by single-particle tracking using the Metamorph software. Single-particle tracking was performed on one bead at a time in 10 zones covering each 80 × 80 μm^2 microscope field analysed. The position of a given bead (x, y coordinates) on each frame was defined as the centroid (geometric centre) of the fluorescent spot corresponding to that bead. To minimize positioning error, image background from the centroid calculation was excluded by setting a brightness threshold. Single bead instantaneous velocities and directions are inferred from 2 consecutive frames. Each bead was tracked during seven frames. The mean bead velocity direction was then calculated for each bead. This operation was repeated in five 80 × 80 μm^2 microscope fields in each of the

DOI: 10.1038/ncb2040

six analysed regions (red circles in Supplementary Information, Fig. S5e) in three different cultures, leading to about 1000 zones analysed. The mean bead velocity directions define the bead propelling directions. We then split the 360° circle into 20° angle windows and scored the number of propelling directions pointing in each 20° slice and represented it in a rose diagram using Matlab.

54. Zhuo, L. *et al.* hGFAP-cre transgenic mice for manipulation of glial and neuronal function *in vivo*. *Genesis* **31,** 85–94 (2001).
55. Marszalek, J. R., Ruiz-Lozano, P., Roberts, E., Chien, K. R. & Goldstein, L. S. B. Situs inversus and embryonic ciliary morphogenesis defects in mouse mutants lacking the KIF3A subunit of kinesin-II. *Proc. Natl Acad. Sci. USA* **96,** 5043–5048 (1999).
56. Morin, X., Jaouen, F. & Durbec, P. Control of planar divisions by the G-protein regulator LGN maintains progenitors in the chick neuroepithelium. *Nature Neurosci.* **10,** 1440–1448 (2007).
57. Gosgnach, W., Messika-Zeitoun, D., Gonzalez, W., Philipe, M. & Michel, J.-B. Shear stress induces iNOS expression in cultured smooth muscle cells: role of oxidative stress. *Am. J. Physiol. Cell Physiol.* **279**, C1880–C1888 (2000).
58. Bailly, E., Doree, M., Nurse, P. & Bornens, M. p34cdc2 is located in both nucleus and cytoplasm; part is centrosomally associated at G2/M and enters vesicles at anaphase. *EMBO J.* **8,** 3985–3995 (1989).
59. Mirzadeh, Z., Merkle, F. T., Soriano-Navarro, M., Garcia-Verdugo, J. M. & Alvarez-Buylla, A. Neural stem cells confer unique pinwheel architecture to the ventricular surface in neurogenic regions of the adult brain. *Cell Stem Cell* **3,** 265–278 (2008).

ERRATUM

Coupling between hydrodynamic forces and planar cell polarity orients mammalian motile cilia

Boris Guirao, Alice Meunier, Stéphane Mortaud, Andrea Aguilar, Jean-Marc Corsi, Laetitia Strehl, Yuki Hirota, Angélique Desoeuvre, Camille Boutin, Young-Goo Han, Zaman Mirzadeh, Harold Cremer, Mireille Montcouquiol, Kazunobu Sawamoto and Nathalie Spassky

Nature Cell Biol. **12,** 341–350 (2010); published online 21 March 2010; corrected after print, 26 March 2010

In the version of this article initially published online and in print, there was an error in the numbering of authors who contributed equally. The corrected numbering should be as follows:

Boris Guirao[1,2,7], Alice Meunier[1,7], Mireille Montcouquiol[6,8], Kazunobu Sawamoto[3,8] and Nathalie Spassky[1,9]

[7,8]These authors contributed equally to this work.
[9]Correspondence should be addressed to N.S. (e-mail: spassky@biologie.ens.fr)

This error has been corrected in both the HTML and PDF versions of the article.

nature cell biology

DOI: 10.1038/ncb2040

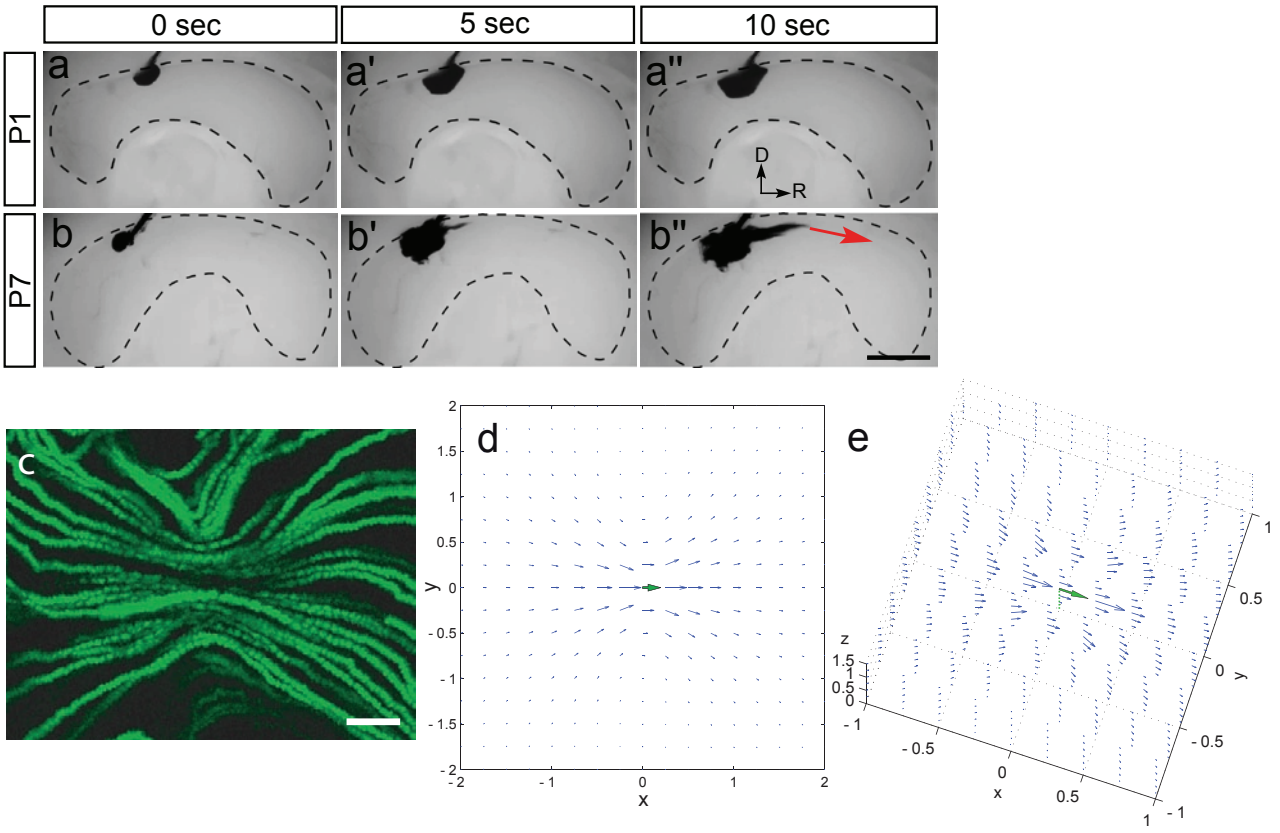

Figure S1 Cilia generated flows. **(a, b)** Ciliary driven ependymal flow emerges postnatally. Fluid flow visualized by movement of India ink drop onto the lateral wall of the lateral ventricle. **(a)** In P1 samples, no directional flow was observed and the stain expands due to ink diffusion in the liquid. **(b)** In P7 samples, ependymal flow becomes clearly directed towards rostral regions (red arrow). Scale bar: 2 mm. **(c-e)** Flow patterns generated by ependymal cells resemble the one created by a single stationary force in the fluid. **(c)** Fluorescent bead trajectories generated by a single ependymal cell observed with a video microscope in a plane ~20 μm above the cell monolayer. Observed bead pathlines are consistent with the flow pattern calculated in (b). This suggests ependymal cell generated flow ~20 μm above cell monolayer is steady and can be described by a steady force acting in the fluid with good approximation as carried out in Ref.[9]. **(d)** Velocity field generated in the (*x, y*) plane (parallel to the surface) by a single steady force *f* in the fluid (green arrows) pointing along the *x* axis at height *h*. Units: *x/L, y/L, L* being the cilium length. Assuming a single cell exerts an average force *f* in the fluid, the flow generated by this cell at distance $d > L$ decreases rapidly as f/d^3 (see Ref.[9] for further details). Hydrodynamic forces upon cilia tend to orient each of them in the flow direction, and can lead to their spontaneous collective alignment or alignment with an external flow, provided that their beat frequency or amplitude are large enough[9]. However, when the distance between cells is too large, hydrodynamic interactions could be too weak to lead to their alignment. This could explain why separate clusters of cells displayed no coherence in their propelling directions as observed here (Fig. 2e and Movie S4). **(e)** 3D velocity field showing the flow generated by this single force. Units: *x/L, y/L*. Scale bar: 6 μm.

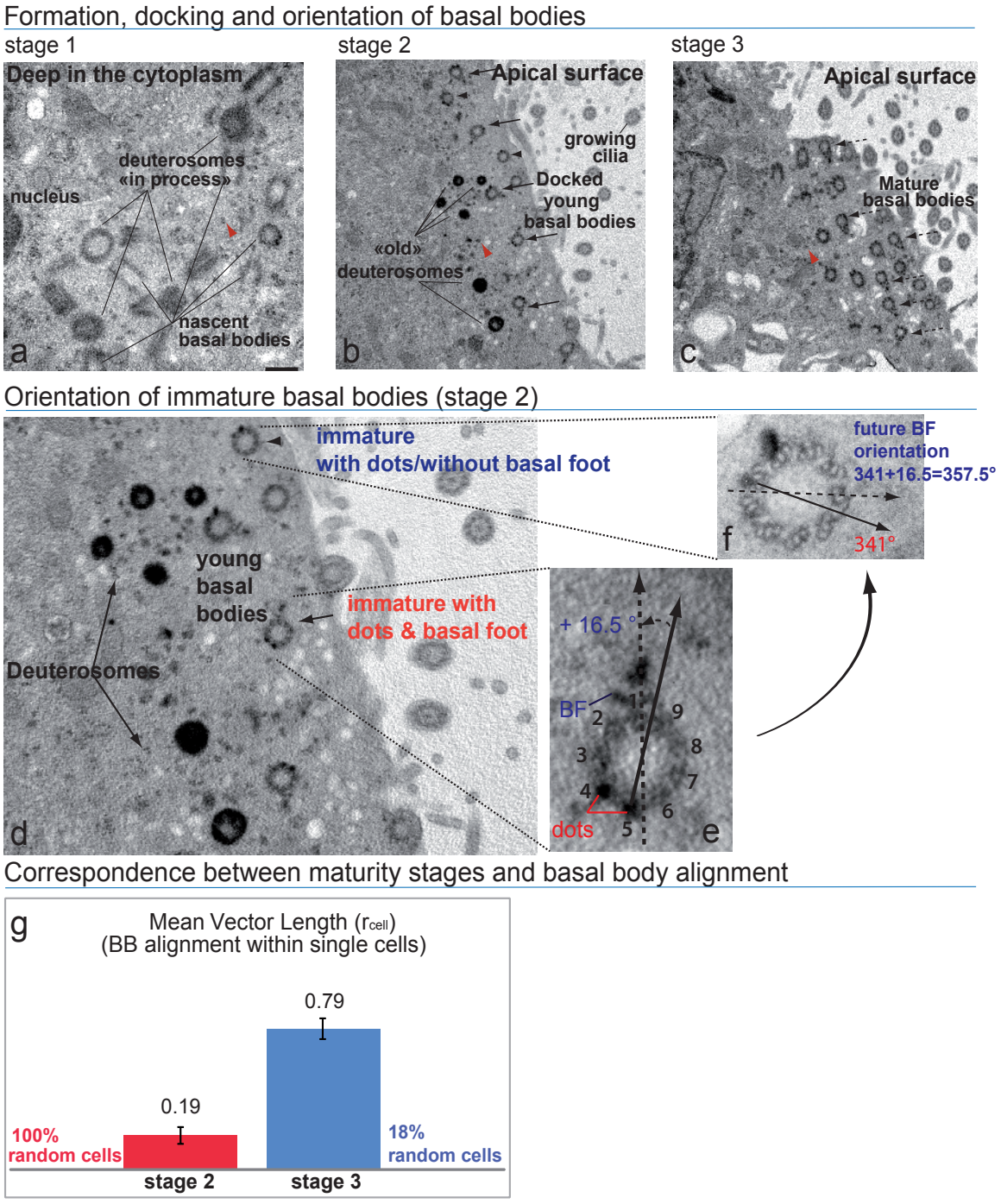

Figure S2 Analysis of young BB orientation. In a P4 ventricle, all ependymal cell maturation stages are observable. We determined three stages of maturation. **(a)** Stage 1 ependymal cells display deuterosomes building BB deep inside the cytoplasm. **(b)** Stage 2 ependymal cells display electron-dense deuterosomes, apically localized, and immature BB docked at the cell surface. At this stage, immature BB exhibit the first sign of asymmetry characterized by electron-dense dots flanking two microtubule triplets (black arrowheads) and some also display a young, faint BF (arrows; see higher magnification in d). **(c)** Stage 3 ependymal cells display mature BB with dark BF (dashed arrows). At this stage, immaturity features (deuterosomes and dots) have disappeared. In allstages, electron dense aggregates are observable in BB vicinity (red arrowheads in a, b, c) as described in Ref.[17]. They are fewer at stage 3 and disappear in mature cells. **(d, e)** Analysis of stage 2 BB with electron-dense dots and faint BF allows us to number microtubule triplets and to show that the position of the electron-dense dots is reproducible (n=35): they flank triplet 4 and 5. The axis that passes through the right dot and between triplet 1 and 9 (thus passing by the BB center ; arrow in e) is at 16,5° +/- 0,5° (n=35) from the axis passing between triplet 5 and 6 and the BF tip (dashed arrow in e), which is the ciliary beating axis. **(f)** We therefore used these asymmetrically positioned dots in order to orient immature BB without BF. By this way we managed to analyze stage 2 cells with more than 20 BB. **(g)** Stage 2 cells display poor BB alignment $\langle r_{Cell} \rangle = 0.19 \pm 0.05$ as compared to stage 3 $\langle r_{Cell} \rangle = 0.79 \pm 0.06$. Moreover, 100% of stage 2 cells display random BB circular distribution as compared to only 18% in stage 3 cells (see Fig. S4 for r_{Cell} definition and random circular distribution criterion). This confirms the progressive ordering of BB throughout development. Scale bar: 0.3 µm in a, 0.7 µm in b,c, 0.25 µm in d, 0.08 µm in e, f.

Docking of immature basal bodies: Serial section of a cell at stage 2

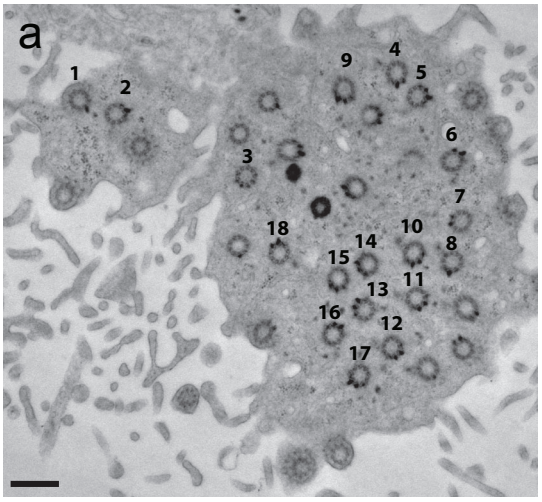

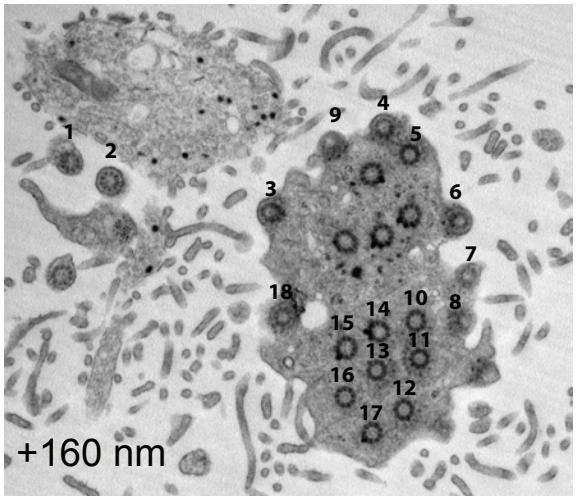

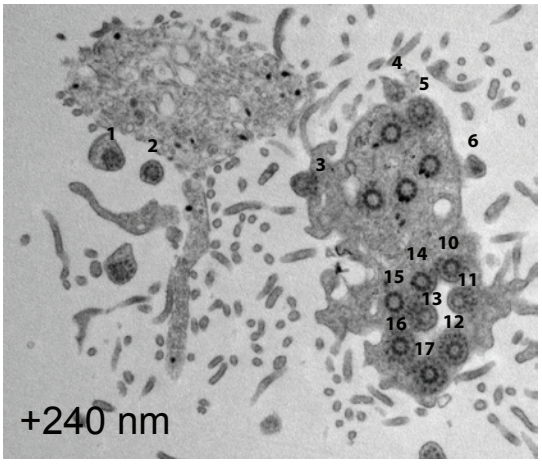

BB number	α dots	α dots + 16,5° = αBF
1	176	192,5
2	231	247,5
3	66	82,5
4	128	144,5
5	217	233,5
6	257	273,5
7	232	248,5
8	113	129,5
9	97	113,5
10	122	138,5
11	149	165,5
12	136	152,5
13	348	4,5
14	36	52,5
15	84	100,5
16	255	271,5
17	74	90,5
18	313	329,5

Basal body orientation in this cell

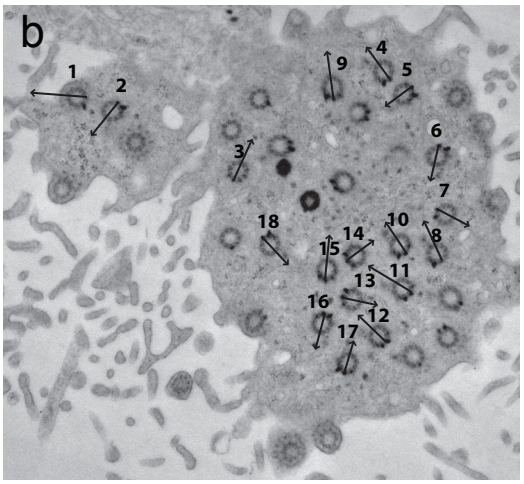

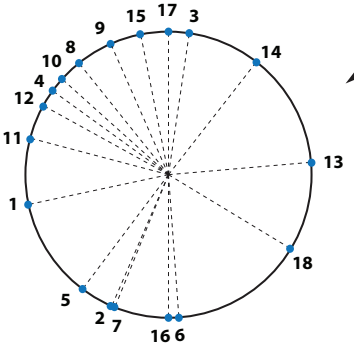

Rayleigh's test: p=0.385
>>> Random distribution

Mean vector length=0.24

Figure S3 BB docking and orientation in a cell at stage 2. **(a)** TEM transverse serial sections of a cell at stage 2 of maturation in a P4 ventricular wall. The numbered BB are the ones for which the transition zone (3 to 18) and/or the growing axoneme (1, 2, 4, 6) appear in one of the section, confirming their docking at the apical cell membrane. **(b)** Example of BB orientation scoring in this cell. These docked BB are then used to assess the level of alignment within young ependymal cells. In this example, 18 docked BB were oriented thanks to the 2 electron dots, as explained in Fig. S2. Scale bar: 1 µm.

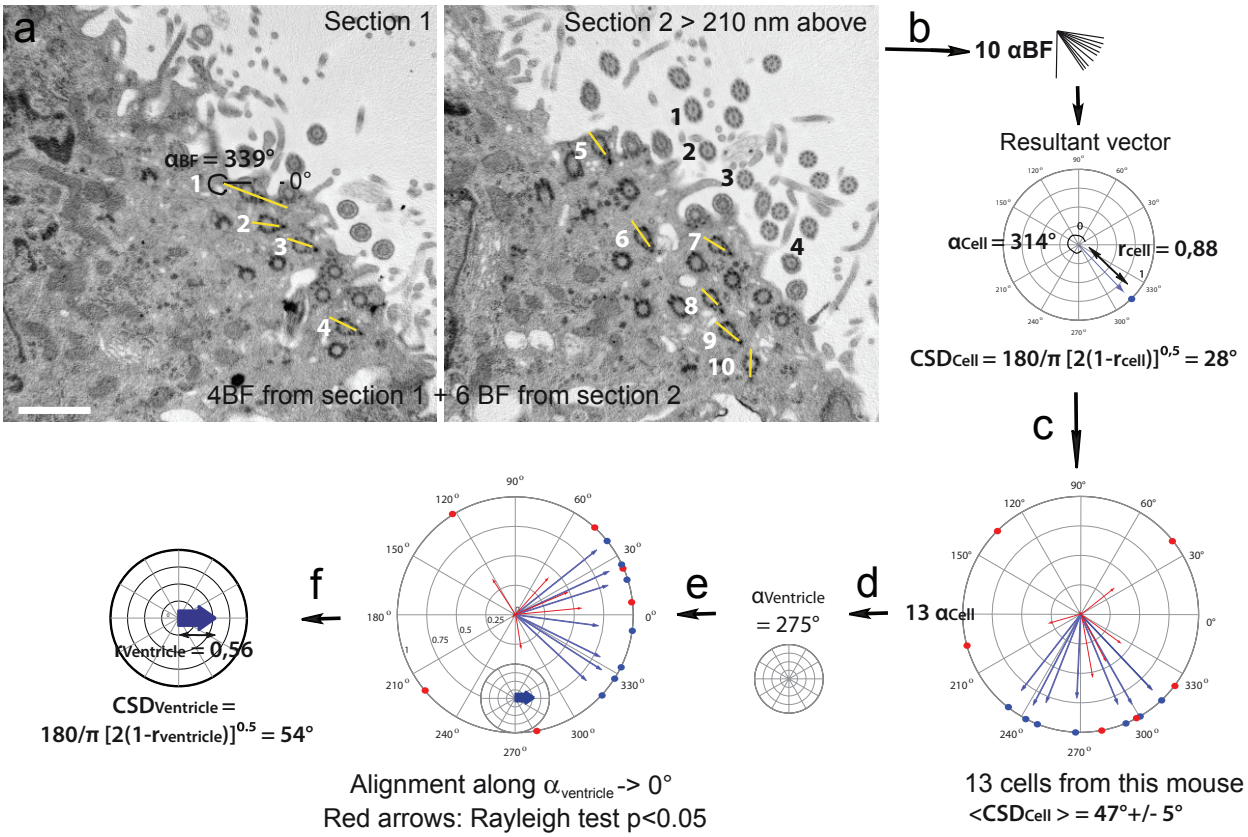

Figure S4 Quantitative analysis of basal foot orientation. Determination of ciliary beating direction within cells was assessed by scoring putative (see Fig. S2) or identified BF polar orientation (pointing toward effective stroke), in TEM sections of ependymal cells from ventricular walls or from *in vitro* cultures. **(a)** For a given cell, BF from 2 to 3 sections (separated from 210 nm) were analyzed. For each sample (ventricular wall or cultured ependymal cells), all section orientations were conserved and systematically aligned before analysis. Therefore, all BF observed in one sample could be oriented relatively to the others. For each cell, the orientation of 6 to 30 BF (α_{BF}) was determined with a mean of 10 BF/cell *in vivo* and 9 BF/cell *in vitro*. **(b)** The angle α_{Cell} and the length r_{Cell} of the resultant mean vector were calculated using ©statistXL software (Broadway, Western Australia) for circular data and plotted on a circular graphic using ©Matlab (The Mathworks, Inc., USA). Arrows point in the BF mean direction within each single cell. Circular standard deviation (CSD_{Cell}) of BF directions within single cells was calculated ($CSD_{Cell} = 180/\pi\ [2(1\text{-}r_{Cell})]^{1/2}$) for each cell. Hence, when BF alignment increases, r_{Cell} increases and CSD_{Cell} decreases. BF circular distributions within each cell were compared to a random distribution using Rayleigh's test and represented with red arrows when found similar. **(c)** 13 vectors corresponding to the 13 cells analyzed in this mouse ventricular wall were represented on the same graphic. **(d)** Using α_{Cell} angles, we calculated the mean ventricular angle $\alpha_{Ventricle}$. **(e)** In order to represent cell vectors of two animals from each analysis on the same graphics, we reset $\alpha_{Ventricle}$ onto 0° for each animal. **(f)** Vector length $r_{Ventricle}$ and ventricular CSD ($CSD_{Ventricle}$) representing the dispersion of "cell directions" (α_{Cell}) within the ventricle were calculated. Likewise, when cell alignment within the ventricle increases, $r_{Ventricle}$ increases and $CSD_{Ventricle}$ decreases. Scale bar: 0.7 µm.

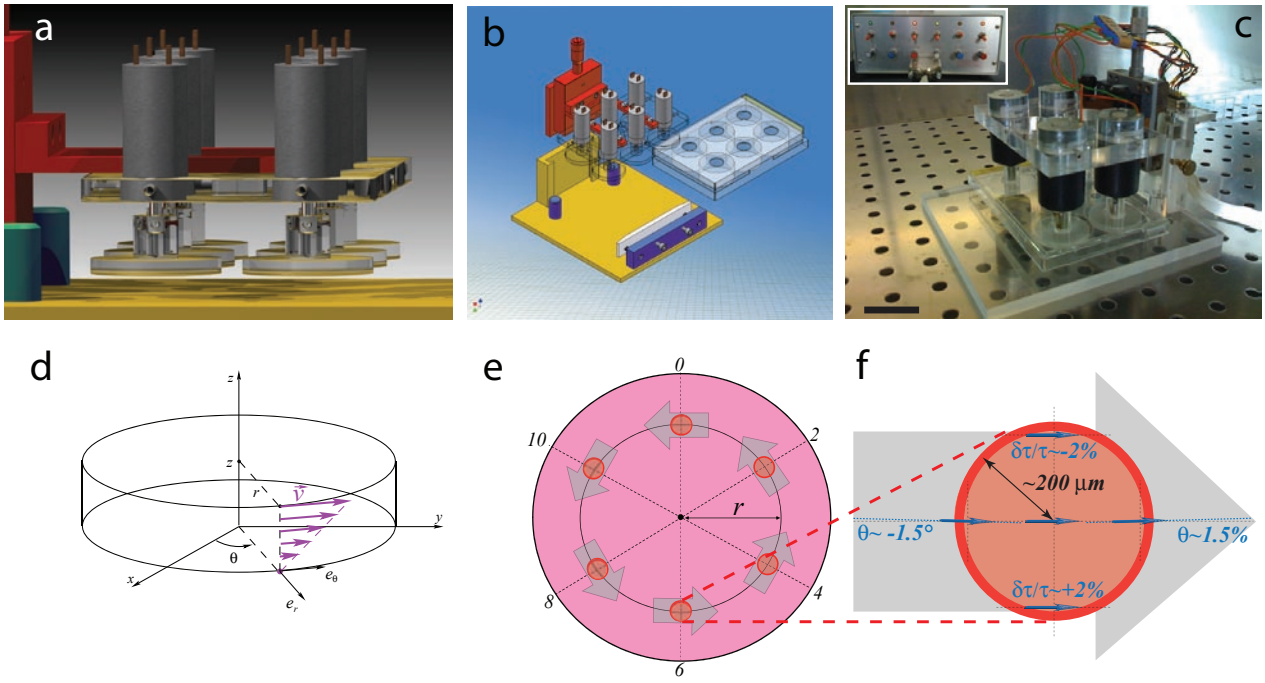

Figure S5 Experimental set up and method of comparative analysis of external flow and bead propelling directions. **(a)** Side view schematic of the experimental set up. Each of the six circular Plexiglas plates is fixed to a rotating motor. The height of the six unit set can vary to adjust the shear stress applied over cells. **(b)** This set up is directly applicable onto classic 6-well plates. **(c)** Picture of the set up used with four motors. Motors are connected to a power supply controlling the rotation speed of each unit independently (inset). This allows the control of the shear stress applied over cells in each well. **(d)** Schematic illustrating the shear flow generated in the culture. The fluid in contact with the rotating plate is dragged at the same speed by its rotation: the generated flow decreases towards the bottom (pink arrows). Velocity and shear stress also vary in the radial direction (increase with *r*): a definite distance from the rotation axis must therefore be chosen to ensure that a similar shear stress was applied in each zone of analysis. **(e)** Zones of analysis and local direction of applied flow. In each culture (pink disc, symbolizing one well) we analyzed six zones (red circles) equally spaced at six different times around the clock and all laying on a $r = 1$ cm circle centered on the rotation axis (centered black point). In each analyzed region, the flow applied during culture is tangential to the 1 cm circle (grey arrows). **(f)** Variations of shear stress (blue arrows) over a zone of analysis (red circle) which is typically ~ 400µm wide. Because of the circular flow generated by the set up, the applied stress τ varies of ±1.5° in direction and ±2% in amplitude as compared to the zone center value. At this scale, the flow can therefore be considered as straight and uniform over the whole zone of analysis. *In vivo*, cilia-powered flow is approximately straight over regions of similar sizes (~ 500µm), but not at the ventricle scale (Fig. 1a, S1 and Ref.[8]), which justifies the relevance of our study.

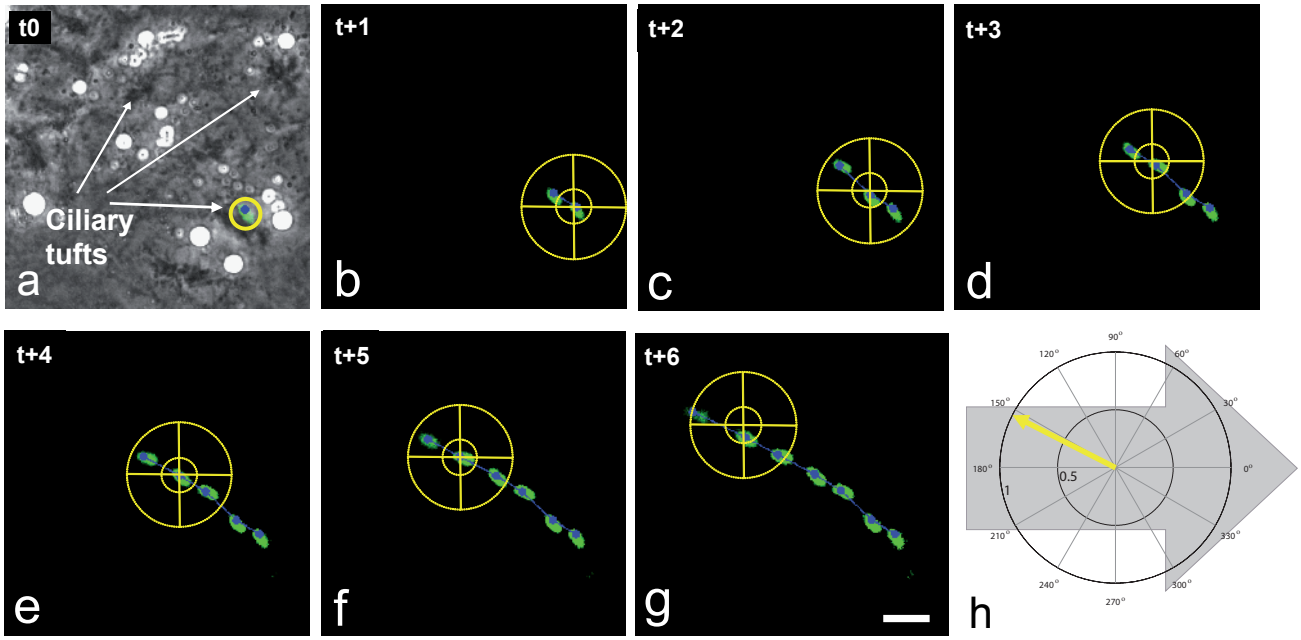

Figure S6 Analysis of beads propelling directions. **(a)** Superposition of phase contrast and fluorescent microscopy images displaying ciliary tufts and one fluorescent bead (green spot circled in yellow). The bright white spots are lipidic droplets. **(b-g)** Single bead tracking technique. Time-lapse sequences of images were acquired using video microscopy to analyze 0.75 µm diameter fluorescent beads movements. Images were first reoriented according to their location in the culture so that the applied flow direction always points horizontally toward the right (thick grey arrow in h). Image background was removed from each frame. The position of a given bead (*x*, *y* coordinates) on each frame was defined as the centroid (geometric center) of the fluorescent spot corresponding to that bead using single-particle tracking tool in *Metamorph* software (yellow targets and blue spots). Bead instantaneous velocity and direction are inferred from two consecutive frames from bead positions in each frame. Single beads were tracked during seven frames. The mean bead velocity direction was then calculated (yellow arrow in h). Time between two frames: 1 s; exposure time: 470 ms per frame. **(h)** The mean velocity direction of the tracked bead is plotted on a polar diagram (yellow arrow). The applied external flow direction in this location of the culture is indicated (thick grey arrow) and compared to the bead mean direction. Same procedure is performed in every analyzed zone leading to statistics on bead propelling direction displayed on polar diagrams in Figs. 2e, h, k, 4h, 5f, and 5h. Scale bar: 10 µm.

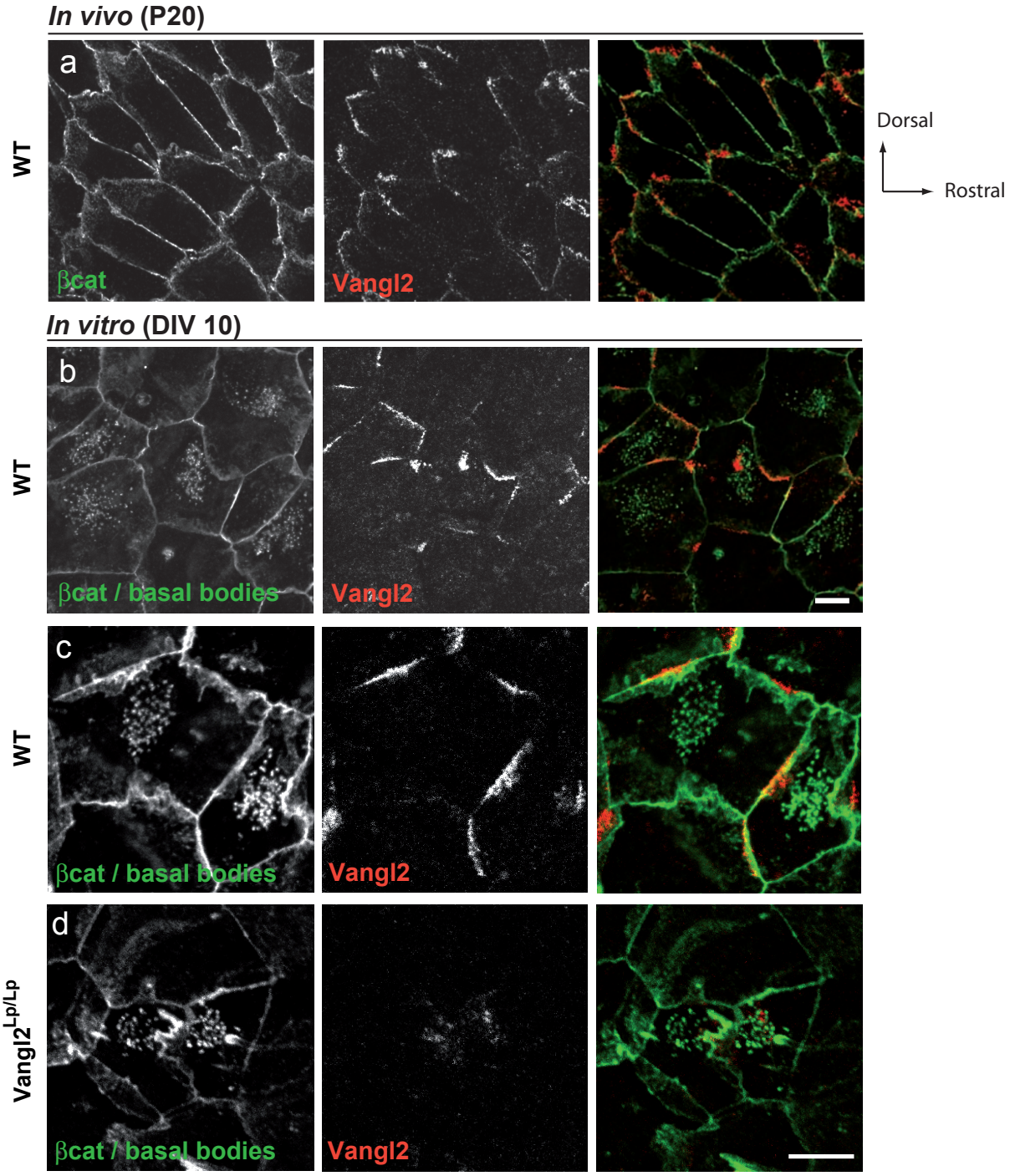

Figure S7 Vangl2 localization at apical cell membrane. **(a, b)** Vangl2 localizes asymmetrically at apical membrane both *in vivo* and *in vitro*. **(a)** Double immunostaining with β–catenin (cell borders, green) and Vangl2 (red) antibodies staining at P20 shows that Vangl2 asymmetric localization colocalizes with caudal cell-cell borders of ependymal cells. **(b)** Triple immunostaining with β–catenin (cell borders, green), CTR453 (BB, green) and Vangl2 (red) shows asymmetric localization of Vangl2 at ependymal cell-cell borders at 10 DIV. Scale bar: 3 μm. **(c, d)** Vangl2 is mislocalized in cultured cells from Vangl2$^{Lp/Lp}$ mice. Triple immunostaining with Vangl2 (red), β–catenin (cell borders, green) and CTR 453 (BB, green) antibodies of WT (c) and Vangl2$^{Lp/Lp}$ mutant (d) multiciliated cells at 10 DIV shows Vangl2 accumulation in cytoplasm aggregates in Vangl2$^{Lp/Lp}$ mutant cells without asymmetric localization at cell-cell borders compared to WT. Scale bar: 7 μm.

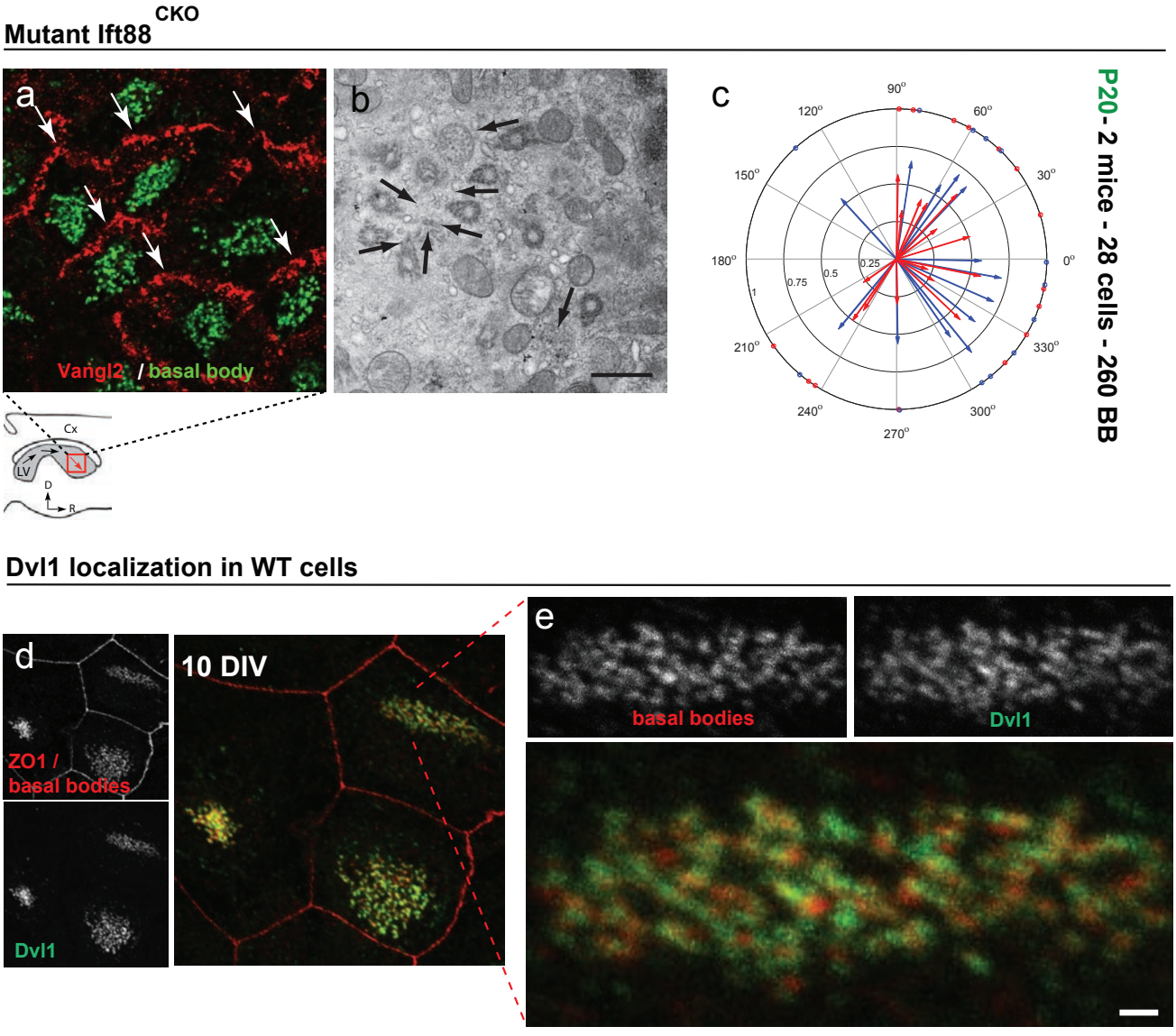

Figure S8 Mutant Ift88^{CKO} phenotype and Dvl1 localization in WT cells. **(a-c)** Ift88^{CKO} ciliary mutant cells display proper apical asymmetric localization of Vangl2 but randomized orientation of basal bodies. **(a)** Double immunostaining with Vangl2 (red), and CTR 453 (BB, green) antibodies shows that Ift88^{CKO} mutant cells display proper Vangl2 asymmetric localization at P20. **(b, c)** TEM of Ift88^{CKO} mutant cells shows impaired orientation of BF pointing in every direction (b) quantified within 28 cells (260 BB) (c). Scale bar: 5 µm in a; 1 µm in b. **(d, e)** The PCP protein Dvl1 is localized in the vicinity of BB in multiciliated ependymal cells at 10 DIV. Triple immunostaining with ZO1 (tight junctions, red), γ-tubulin (BB, red) and Dvl1 (green) antibodies of multiciliated ependymal cells at 10 DIV shows that Dvl1 is localized in the vicinity of BB. Scale bar: 3 µm in d; 0.5 µm in e.

Supplementary Movie Legends

Movie S1 Fluorescent bead movements in a 5 DIV wild type ependymal cell culture. Multiciliated cells are sparsely distributed and propel green fluorescent beads coming nearby mildly and in every direction. White dashed circles indicate beating ciliary tufts. Yellow arrows indicate local propelling directions. Time-lapse series of superposed phase contrast and fluorescent video-microscopy images is first shown, followed by progressive sum of 100 fluorescent video-microscopy images allowing to visualize bead trajectories. Each movie is played twice for visualization convenience. Motionless beads were removed. The white spots are lipidic droplets.

Movie S2 Fluorescent bead movements in a 10 DIV wild type ependymal cell culture. By 10 DIV, cultures display many more ciliated cells that propel beads more powerfully as compared to 5 DIV cultures. Cells are arranged in clusters (group of adjacent white dashed circles) propelling beads in a common direction (yellow arrows). These propelling patterns suggest spontaneous alignment of cell propelling direction at cluster scale due to hydrodynamic interactions between cells as proposed in Ref. [9]. See Movie S1.

Movie S3 Fluorescent bead movements in a 10 DIV culture where external flow was applied during 5-10 DIV. Cells clearly propel fluorescent beads toward the left coinciding with the direction of the flow applied during growth. Quantitative analysis of beads propelling directions confirms this effect (Fig. 2d) showing that cilia of immature cells have the ability to respond to hydrodynamic forces by orienting in the applied flow direction. See Movie S1.

Movie S4 Fluorescent bead movements in a 10 DIV control culture. In contrast to cultures shown in movie S3, no external flow was applied during growth here. Cultures display typical clusters of cells propelling beads roughly in the same direction at cluster scale, but without correlation between two separate clusters (compare arrow directions in upper and lower groups). Note that conditions of culture are similar to movie S2. See Movie S1.

Movie S5 Fluorescent bead movements in a 15 DIV where external flow was applied during 10-15 DIV. Observed flow patterns look very similar to control cultures where no flow was applied (see movie S4): clusters of cells propel beads in one common direction at cluster scale but with no correlation between clusters, as confirmed by quantitative analysis (Fig. 2h). This shows that mature cells have lost their ability to respond to hydrodynamic forces and orient with the external flow. See Movie S1.

Movie S6 Vangl2 immuno-localization in P20 ventricular wall. Z-stack (15 µm) of a double immunostaining with Vangl2 (red) and a cilia marker (TAP, green) antibodies showing ciliary and apico-caudal localization of Vangl2 in P20 ventricular wall. Upper left panel shows Vangl2 staining and Lower left panel shows cilia staining.

Movie S7 Ciliary beatings in mature wild type cultures. The flow direction is indicated by fluorescent bead movement. Time-lapse series of superposed phase contrast and fluorescent video-microscopy images. The white spots are lipidic droplets.

Movie S8 Ciliary beatings in mature Vangl2$^{Lp/Lp}$ cultures. Ciliary beatings and bead propulsion appear very similar to wild type cultures suggesting Vangl2 is not involved in ciliary beating. This is confirmed by measures of bead mean velocities in wild type and Vangl2$^{Lp/Lp}$ cultures that are found very similar as well ($\langle V_{WT} \rangle = 8.3 \pm 0.3$ µm/s ($n = 166$) and $\langle V_{Vangl2KO} \rangle = 7.8 \pm 0.3$ µm/s ($n = 278$) ; mean ± s.d.). This strongly suggests Vangl2$^{Lp/Lp}$ single cilia have normal beating pattern. See movie S6.

Movie S9 Fluorescent bead movements in a 10 DIV culture of Vangl2$^{Lp/Lp}$ cells where external flow was applied during 5-10 DIV. Despite the directed flow applied during growth, Vangl2$^{Lp/Lp}$ cells propel beads in every directions, similarly to controls. Unlike wild type cultures, even adjacent cells propel beads in random directions and no clusters of cell propelling beads coherently can be observed. These results shows Vangl2$^{Lp/Lp}$ cells cannot respond to hydrodynamic forces and orient with the flow. See Movie S1.

Movie S10-S12 Fluorescent bead movements in a P20 lateral ventricle wall electroporated with GFP-Vangl2^{Lp}. Cells successfully electroporated with the GFP-Vangl2^{Lp} construct appear in green. Red beads display a smooth directed flow in the caudo-rostral direction except in the vicinity of electroporated cells where propulsion occurs in every direction. Green beating cilia can be observed showing presence of GFP-Vangl2^{Lp} at cilia, consistently with WT Vangl2 ciliary localization. Time-lapse series of fluorescence video-microscopy images is shown, followed by progressive sum of 100 images enabling to visualize bead trajectories. Each movie is played twice for visualization convenience. White arrows indicate normal caudo-rostral flow direction while yellow arrows point in every direction illustrating the random beating directions of cells electroporated with GFP-Vangl2^{Lp}. Each movie was performed in a different animal.

Movie S13-S14 Fluorescent bead movements in a P20 lateral ventricle wall electroporated with GFP. As opposed to GFP-Vangl2^{Lp} electroporated cells, GFP electroporated cells (in green) propel beads in the same caudo-rostral direction as their neigbhoring cells (white arrows). Each movie was performed in a different animal